



1 The role of fault network geometry on the complexity of 2 seismic cycles in the Apennines

3 Constanza Rodriguez Piceda¹, Zoë K. Mildon¹, Billy J. Andrews¹, Yifan Yin², Jean-Paul
4 Ampuero³, Martijn van den Ende³, Claudia Sgambato⁴, Percy Galvez⁵

5 ¹ University of Plymouth, School of Geography, Earth and Environmental Sciences, Plymouth, PL4 8AA,
6 United Kingdom

7 ² MIT Department of Earth, Atmospheric and Planetary Science, Cambridge, MA 02139, United States

8 ³ Université Côte d'Azur, Observatoire de la Côte d'Azur, IRD, CNRS, Géoazur, Valbonne, 06905, France

9 ⁴ Birkbeck University of London, London, WC1E 7HX, United Kingdom

10 ⁵ Everest Group, Zürich, CH-8001, Switzerland

11 *Correspondence to:* constanza.rodriguezpiceda@plymouth.ac.uk

12

13 **Abstract.** Estimating the recurrence intervals and magnitudes of earthquakes for a given fault is essential for
14 seismic hazard assessment but often challenging due to the long recurrence times of large earthquakes. Fault
15 network geometry (i.e. spatial arrangement between faults) plays a key role in modulating stress interactions and,
16 consequently, earthquake recurrence and magnitude. Here, we investigate these effects of fault network geometry
17 using earthquake cycle models to generate numerous earthquakes on two different networks of normal faults in
18 Italy: the Central Apennines, characterised by a wide network of faults offset across strike, and the Southern
19 Apennines, a narrow fault network where faults are predominantly arranged along strike. For each region, we ran
20 an earthquake cycle simulation on systems of seven normal faults generating approximately 150 earthquakes. In
21 the Central Apennines, co-seismic stress transfer between faults promotes more heterogeneous stress, more partial
22 ruptures, greater M_w variability and less periodic behaviour of large earthquakes (coefficient of variation of
23 recurrence time, CV 0.1-0.9). In contrast, faults in the Southern Apennines experience more homogeneous stress
24 loading, leading to a higher proportion of full-fault ruptures with more regular recurrence intervals (CV 0-0.4). In
25 both fault networks, high long-term slip rate amplifies the effects of fault interactions: faults with higher long-
26 term slip rate are more sensitive to positive stress perturbations from nearby faults compared to slower-moving
27 faults. These results highlight that incorporating stress interactions from fault network geometry into seismic
28 hazard models is particularly important for networks of faults offset across strike, where rupture behaviour is more
29 variable.

30 1 Introduction

31 Earthquake recurrence intervals and magnitude distributions are key inputs for probabilistic and time-dependent
32 seismic hazard assessment (Gerstenberger et al., 2020), therefore determining the mechanisms behind their
33 variability is necessary to effectively mitigate associated risks. Fault stress interactions, which occur as stress is



34 redistributed following earthquakes (Harris and Simpson, 1998; King et al., 1994; Stein, 1999), influence the
35 recurrence and magnitude of earthquakes. These interactions can be either permanent (Coulomb static stress
36 transfer, CST) or transient (associated with seismic wave propagation; Freed, 2005), and may either promote or
37 inhibit rupture depending on the relative location and orientation of faults (e.g., Harris and Simpson, 1998; King
38 et al., 1994; Nicol et al., 2005; Stein, 1999).

39 Several studies have investigated how fault network geometry shapes stress interactions (Cowie et al., 2012;
40 Rodriguez Piceda et al., 2025a; Sgambato et al., 2020a, 2023). In particular, here we distinguish two basic spatial
41 arrangements of fault networks: “along-strike fault networks” in which faults are co-planar, aligned in the along-
42 strike direction, and “across-strike fault networks” in which faults are non-co-planar, offset in the across-strike
43 direction. Sgambato et al. (2020, 2023) used CST analysis of historical earthquakes in Italy to show that faults
44 with more across-strike interactions develop more irregular stress loading histories, less dominated by interseismic
45 stress loading, whereas faults with fewer across-strike interactions tend to have more regular stress histories
46 controlled by interseismic loading. While these patterns suggest a link between stress loading history and the
47 regularity of earthquake recurrence, it remains difficult to isolate the effects of network geometry using historical
48 data alone, since other processes such as dynamic stress transfer from seismic waves, postseismic stress
49 redistribution and fluid pressure changes (Freed, 2005) can obscure stress patterns driven by network geometry.

50 To explore the effects of network geometry under controlled conditions, numerical modelling approaches have
51 been employed. For instance, studies with elastic-brittle lattice models (e.g., Cowie et al., 2012) found that more
52 across-strike interactions lead to shorter earthquake recurrence intervals. However, these models do not include
53 the effects of time-dependent stress healing and frictional memory as observed in natural fault rocks (Marone,
54 1998b), resulting in less realistic stress-loading histories, nor they address the effects of fault geometry in
55 earthquake magnitudes and the partition between seismic and aseismic slip modes.

56 These effects are accounted for in models of sequences of earthquakes and aseismic slip (SEAS), incorporating
57 rate-and-state friction, enabling a more realistic representation of nucleation, healing and slip mode variability
58 (Erickson et al., 2020; Jiang et al., 2022; Lapusta et al., 2000; Rice, 1993). For example, Romanet et al., (2018)
59 modelled two partially overlapping strike-slip faults with equal long-term tectonic slip rate and found that smaller
60 across-strike separations can produce complex earthquake sequences and slow slip events. Yin et al. (2023)
61 extended this to three overlapping strike-slip faults, showing that fault interactions promote aperiodic cycles and
62 partial ruptures (i.e. ruptures that do not break the whole fault). Rodriguez Piceda et al. (2025) focussed on the
63 role of along-strike and across-strike separation on the earthquake cycle using a simplified system of two parallel
64 normal faults with identical loading conditions. They showed that across-strike separation has a greater impact on
65 recurrence intervals than along-strike separation, with closer across-strike faults characterised by more complex
66 and non-periodic seismic cycles.

67 Natural fault networks, however, are geologically more complex than in generic models: they are often formed
68 by more than three faults, are more geometrically diverse, and long-term slip rates vary between faults (e.g. Nicol
69 et al., 2016; Papanikolaou et al., 2005; Papanikolaou and Roberts, 2007; Roberts, 2007; Roberts and Michetti,
70 2004). The combined effect of such complexities on earthquake timing, magnitude and slip modes remains poorly



understood, as does the role of slip rate in modulating interaction effects. These research gaps have direct implications for seismic hazard assessment.

Here we address these questions by introducing a novel approach developing 3D SEAS simulations of over 100 earthquakes based on the Southern and Central Apennines normal-fault networks in Italy, an ideal natural laboratory due to its diverse network geometries and fault slip rates constrained by field data (Faure Walker et al., 2021; Mildon et al., 2019; Sgambato et al., 2020b) and exceptional historical and paleoseismic records (Galadini and Galli, 1996, 1999; Galli, 2020; Galli et al., 2015; Guidoboni et al., 2019; Pantosti et al., 1993; Rovida et al., 2020). This approach overcomes several of the simplifications of previous studies by combining realistic fault network geometries, field-derived loading rates and spontaneous rupture propagation within a continuum framework. We investigate the effects of network geometry and long-term slip rate on earthquake recurrence, magnitude distributions, and slip behaviour, and discuss the implications for incorporating such variability into time-dependent seismic hazard models.

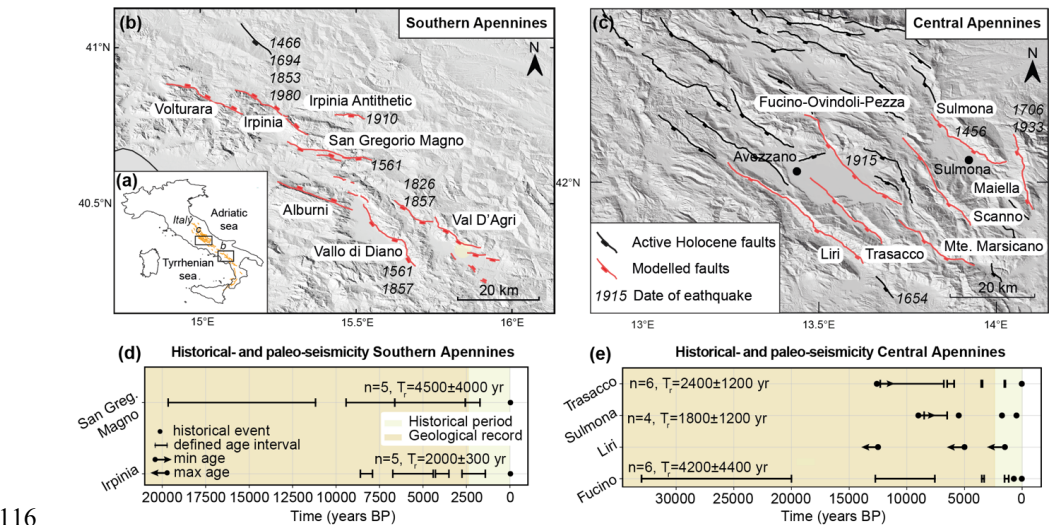
2 Geological background

The Apennines fold-and-thrust belt developed during the Neogene and Quaternary due to the convergence between the Eurasian and African plates (Anderson and Jackson, 1987; Doglioni, 1993; Jolivet et al., 1998). The thrusting phase was followed by extensional tectonics during the Pliocene (~2-3 Ma; Cavinato & Celles 1999; Roberts & Michetti 2004). This extensional phase, continuing to the present day, led to the formation of NW-SE oriented normal faults that run nearly parallel to the fold-and-thrust belt. The tectonically active faults have formed surface offsets preserved since the Last Glacial Maximum (12-18 Ka), allowing the estimation of throw rates from exposed Holocene fault scarps (Papanikolaou and Roberts, 2007; Roberts and Michetti, 2004). In the Southern Apennines, average throw rates on individual faults range between 0.2 and 0.67 mm/yr (Faure Walker, 2010; Papanikolaou and Roberts, 2007; Roberts and Michetti, 2004; Sgambato et al., 2020a, b), while in the Central Apennines, they range between 0.2 and 1.56 mm/yr (Faure Walker et al., 2009; Faure Walker, 2010; Faure Walker et al., 2019a, 2021; Mildon et al., 2019; Papanikolaou and Roberts, 2007; Roberts and Michetti, 2004). The different slip rates among faults allowed us to assess how slip rates modulate or amplify stress transfer and interaction between faults.

A subset of faults in the Southern and Central Apennines was chosen for computational efficiency. The chosen fault networks differ in the number, length and orientation of faults. The chosen sector in the Central Apennines is characterised by a wide fault network, with up to 8 faults arranged NW-SE (Fig. 1b), whereas the Southern Apennines has a narrower fault network with fewer faults accommodating the extension, with a maximum of 3 across-strike faults (Fig. 1c). These faults are associated with moderate to large magnitude earthquakes (M_w 5.5-7; e.g., Bagh et al., 2007; Chiaraluce et al., 2005, 2022; Guidoboni et al., 2019). In the Southern Apennines, the historical record documents 9 earthquakes of $M_w > 5.6$ since 1466 associated with the studied faults (Fig. 1c, Table B1; Cello et al., 2003; Galli et al., 2006, 2014; Galli and Peronace, 2014; Giardini et al., 1996; Rovida et al., 2020; Westaway, 1993; Westaway and Jackson, 1987). Two multi-fault seismic sequences have occurred in the region: one in 1857 of estimated M_w 7.1 involving either the Vallo di Diano and the Val D'Agri faults (Benedetti et al., 1998; Cello et al., 2003; Galli et al., 2006) or the Caggiano-Montemurro fault (Bello et al., 2022); and a second in 1980 of M_w 6.81 that ruptured the Irpinia (also known as Monte Marzano fault, e.g., Galli, 2020), and Irpinia



109 antithetic faults, as well as possibly the San Gregorio fault (Sgambato et al., 2025). This rupture included a
110 northeast dipping segment of the Irpinia fault known as the Pantano di San Gregorio segment (D’Adezzio et al.,
111 1991, Fig. 1b). The 1980 event was the largest earthquake instrumentally recorded in the Apennines (Bernard and
112 Zollo, 1989). In the studied segment of the Central Apennines, the historical record includes 7 earthquakes of
113 $M_w > 5.6$ since 1456 associated with the studied faults, including the 1915 A.D Fucino earthquake. Paleoseismic
114 data is available for 1 and 4 of the modelled faults in Southern and Central Apennines, respectively (Fig. 1d-e,
115 Table B2).



117 **Figure 1: (a) Location of selected fault regions in Italy; (b-c) Map of the fault regions in the Apennines and**
118 **historical earthquakes (post 1400AD). Active Holocene fault traces in the (b) Southern Apennines (based**
119 **on Sgambato et al., 2020b) and (c) Central Apennines (based on Faure Walker et al., 2021), showing the**
120 **different fault network geometries between the regions, with few across-strike faults in the Southern**
121 **Apennines and multiple across-strike faults for Central Apennines. Dashed black lines show the debated**
122 **link between Vallo di Diano and Auletta faults and Auletta and Caggiano-Montemurro faults (see section**
123 **3.1). (d-e) Chronology of paleoseismic and historical events with $M > 6$ in modelled faults of the (d) Southern**
124 **Apennines and (e) Central Apennines (see Table B2 for details; (Galadini and Galli, 1999; Galli et al., 2008,**
125 **2015, 2016; Pace et al., 2020; Pantosti et al., 1993). Whisker plots represent the estimated time range of**
126 **seismic events. The number of paleoseismic events per fault with defined aged brackets (n), and their**
127 **estimated mean and standard deviation of recurrence time (T_r) is also shown.**

128 3 Methods

129 3.1 Model set-up

130 We use the boundary-element software QDYN (Luo et al., 2017) to model SEAS on the Southern and Central
131 Apennines fault networks, each composed of 2D normal faults governed by rate-and-state friction, embedded in
132 a 3D elastic medium (see Appendix A for a description of the governing equations).



We model 7 faults in the Southern Apennines (Alburni, Irpinia, Irpinia Antithetic, San Gregorio Magno (here referred as “San Gregorio”), Val D’Agri, Vallo Di Diano and Volturara faults (Fig. 2a)) and 7 faults in the Central Apennines (Fucino-Ovindoli-Pezza (here referred as “Fucino”, also known as San Benedetto dei Marsi-Goia dei Marsi segment by Galadini and Galli (1999)), Liri, Maiella, Monte Marsicano, Scanno, Sulmona (also known as Monte Morrone fault by Galli et al. (2015)) and Trassaco faults (Fig. 2b)). All selected faults are active, with documented Holocene throw (Faure Walker et al., 2021; Sgambato et al., 2020a; Valentini et al., 2017). For computational reasons and to ensure numerical stability arising from fault intersections, we exclude three active faults in the Central Apennines from the model (Parasano-Pescina, Tremonti and San Sebastiano faults). Tremonti and Parasano-Pescina faults are relatively short (<10 km), while the San Sebastiano fault exhibits a maximum Holocene slip rate of 0.37 mm/yr, much slower than the other faults in the network, which range from 1.08 to 1.99 mm/yr (Papanikolaou et al., 2005; Roberts and Michetti, 2004). These three faults are likely to have a minor contribution to the regional seismic hazard and therefore can be excluded from our models.

The trend and average dip of each fault is taken from published sources (Fault2SHA database, Faure Walker et al. (2021); Mildon et al., (2019); and Sgambato et al., 2020b) (Table 1). For the Central Apennines, we use the definition of “main fault traces” of Fault2SHA, which represent how faults segments have been interpreted to be linked at depth, at the scale recommended for input into hazard models (Faure Walker et al., 2021). For the Southern Apennines, which are not covered by the Fault2SHA database, we utilise fault traces from Sgambato et al., (2020b). The geometry and extent of some of these fault traces is debated. For instance, in some interpretations the NW segment of Vallo di Diano fault (also known as Auletta fault or Caggiano fault) is a separate segment from this fault and continues SE (Galli et al., 2006) or even joins with Val D’Agri fault as part of the Caggiano-Montemurro fault system (Bello et al., 2022) (Fig. 1b). Here, we follow the interpretation of Sgambato et al. (2020b), where the NW segment is part of Vallo di Diano fault based on the field-based evidence of the slip vector orientations (Papanikolaou and Roberts, 2007).

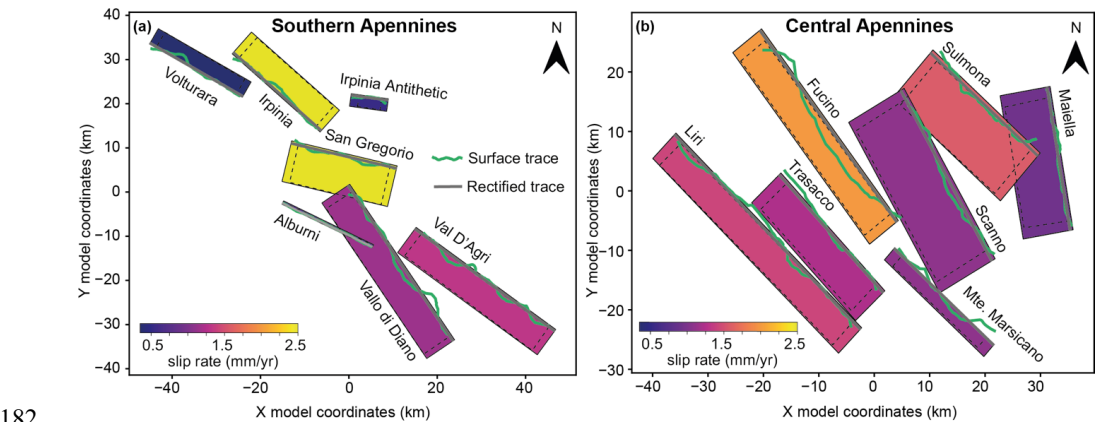
To accommodate QDYN current restriction to a uniform strike for each dip-slip fault, we rectify the fault traces (Fig. 2). The fault depths are set in most of the cases to 15 km, which is taken as approximately the depth of the brittle-ductile transition and is consistent with hypocentral depths observed in the region (Chiarabba et al., 2005; Chiaraluce et al., 2005; Frepoli et al., 2011). We make two exceptions for fault geometry parameters. The Irpinia Antithetic fault, being relatively short (length < 15 km), is assigned a depth of 8 km to maintain an aspect ratio of 1 (Nicol et al., 1996). This modification has implications for the generation of full ruptures, as addressed in the Results and Discussion sections. We limited the Alburni fault to a depth of 3 km to prevent numerical instabilities caused by the intersection with the Vallo di Diano fault. This approximation may lead to an underestimation of its potential involvement in multi-fault rupture sequences and stress transfer, especially near the Vallo di Diano fault. However, the Alburni fault is not thought to have ruptured in historical times, but it is considered to have been active between late Pliocene and late Pleistocene (Gioia et al., 2011; Soliva et al., 2008).

We assign a constant loading rate value to each fault, corresponding to the maximum Holocene slip-rate (Figure 2; Cinque et al., 2000; Faure Walker, 2010; Faure Walker et al., 2019, 2021; Galli et al., 2014; Morewood and Roberts, 2000; Papanikolaou et al., 2005; Roberts and Michetti, 2004; Valentini et al., 2017). Preliminary trials conducted in this study and from previous work (e.g., Yin, 2022), show that in the LSODA solver used here slip



171 rates below 1 mm/yr can cause velocity values to drop below numerical precision, especially when neighbouring
172 faults also exhibit low slip rates. Therefore, to keep numerical stability, we scale up the loading rate by a factor
173 of 100. Based on these trials and on previous studies we find that this scaling has minimal impact on seismicity
174 statistics, once we correct simulations outputs (such as recurrence times) for this upscaling factor (see Appendix
175 B). All time scales reported hereafter account for this correction factor.

176 The set up does not contain further complexities such as variable fault geometry, heterogeneous slip-rate
177 distribution along the fault strike, and heterogeneous distribution of frictional properties. Although these elements
178 may generate heterogeneous stress concentrations that might act as barriers to rupture propagation or as regions
179 of earthquake nucleation (Delogkos et al., 2023; Hillers et al., 2007; Luo and Ampuero, 2018; Mildon et al., 2019),
180 we chose to omit these complexities to primarily focus on the impact of fault network geometry and fault stress
181 interactions on rupture dynamics.



182
183 **Fig. 2: Map view of the model geometry for the (a) Southern Apennines and (b) Central Apennines fault**
184 **network. Fault planes are colour-coded according to their Holocene slip rate. Black dashed lines show the**
185 **velocity-weakening asperities. Surface fault traces (green) derived from (Faure Walker et al., 2021; Mildon**
186 **et al., 2019; Sgambato et al., 2020b) and rectified traces (grey) used in the model are also shown.**

187
188 **Table 1: Geometry and long-term slip rate of modelled fault sources in the Southern and Central Apennines.**
189 References for slip rate: [1] (Valentini et al., 2017) [2] (Faure Walker, 2010) [3] (Galli et al., 2014) [4] (Cinque
190 et al., 2000) [5] Fault2SHA database (Faure Walker et al., 2021) [6] (Morewood and Roberts, 2000) [7] (Roberts
191 and Michetti, 2004) [8] (Faure Walker et al., 2019a) [9] (Papanikolaou et al., 2005)

Modelled region	Fault	Map trace length (km)	Average fault dip (deg)	Maximum long-term slip rate (mm/yr)
-----------------	-------	-----------------------	-------------------------	-------------------------------------



Southern Apennines	Alburni fault	23	74	0.7 [1] [2]
	Irpinia fault	27	66	2.5 [1] [3]
	Irpinia Antithetic fault	8.5	70	0.53 [1] [2]
	San Gregorio fault	24	58	2.5 [1] [3]
	Val D'Agri fault	39	64	1.3 [1] [2]
	Vallo Di Diano fault	42	63	1.15 [1] [4]
	Volturara fault	24	75	0.35 [1] [2]
Central Apennines	Fucino fault	40	66	1.99 [5] [6]
	Liri fault	47	68	1.41 [5] [7]
	Maiella fault	24	58	0.92 [5] [7]
	Monte Marsicano fault	24	7	1.08 [5] [7]
	Scanno fault	33	52	1.08 [5] [8]
	Sulmona fault	26	54	1.57 [5] [9]
	Trasacco fault	27	64	1.22 [5] [7]



193 The simulations run for 11 kyrs to ensure a sufficient number of seismic events for statistical analysis, with the
194 first 500 years discarded as the spin-up phase. To compute the duration of a seismic event, we consider that it
195 starts when one fault element has a slip rate larger than 0.1 m/s and stops when the slip rate of all the elements
196 slip drops below 0.01 m/s.

197 We additionally simulate SEAS on each individual isolated fault included in the Southern and Central Apennines
198 networks to determine their reference behaviour in the absence of stress interactions with other faults. These
199 simulations use the same parametrization as the full fault network simulations described above.

200 3.2 Fault network and seismic cycle characteristics

201 To quantify the effect of across-strike faults, we compute an across-strike interaction index (AI) for each fault i
202 as:

$$203 \quad AI_i = \sum_{j \neq i} \frac{1}{s_{ij}} \quad (1)$$

204 where j are the indices of other across-strike faults, s_{ij} is the across-strike separation between fault i and fault j
205 (see Appendix C for a detailed definition of the separation between faults). The inverse weighting $\frac{1}{s_{ij}}$ ensures that
206 faults that are closer contribute more to the index than those farther away. Faults with a larger number of across-
207 strike interactions have a higher across-strike interaction index. We focus on across-strike density since previous
208 work (Rodriguez Picada et al., 2025) showed that across-strike interactions dominate over along-strike
209 interactions at comparable distances.

210 To characterise the complexity of seismic cycles, we compute three metrics: the coefficient of variation of
211 recurrence times of individual faults (CV_{Tr}), the normalised number of partial ruptures (N_p') and the coefficient
212 of variation of rupture lengths (CV_{RL}).

213 CV_{Tr} is calculated as:

$$214 \quad CV_{Tr} = \frac{std(T_r)}{mean(T_r)} \quad (2)$$

215 where T_r is the distribution of time intervals between consecutive events on the same fault. $CV_{Tr} = 0$ indicates
216 strictly periodic seismic cycles; $0 < CV_{Tr} < 0.5$, strongly periodic; $0.5 \leq CV_{Tr} \leq 1$, weakly periodic; $CV_{Tr} = 1$ indicates
217 that event timing is random and independent of other events; and $CV_{Tr} > 1$ implies event clustering (Boschi et al.,
218 1995).

219 N_p' is calculated as:

$$220 \quad N_p' = \frac{N_p}{N (W_s/L_\infty)} \quad (3)$$

221 where N_p is the number of partial ruptures, N the total number of events for each fault, W_s the seismogenic width
222 and L_∞ the nucleation length (Eq. A5) introduced by Rubin and Ampuero (2005)(Rubin and Ampuero, 2005).



223 CV_{RL}' is calculated as:

224
$$CV_{RL}' = \frac{(std(RL)/mean(RL))}{(W_s/L_\infty)} \quad (4)$$

225 where RL is the distribution of rupture lengths.

226 Both N_p' and CV_{RL}' are normalised by W_s/L_∞ to account for fault-to-fault differences in seismogenic width W_s
227 and the nucleation length L_∞ , enabling comparison of partial ruptures and rupture length variability (Cattania,
228 2019; Barbot, 2019). Overall, faults with larger CV_{T_r} , N_p' , CV_{RL}' have seismic cycles characterised by less periodic
229 recurrence, more frequent partial ruptures and a wider range of rupture sizes.

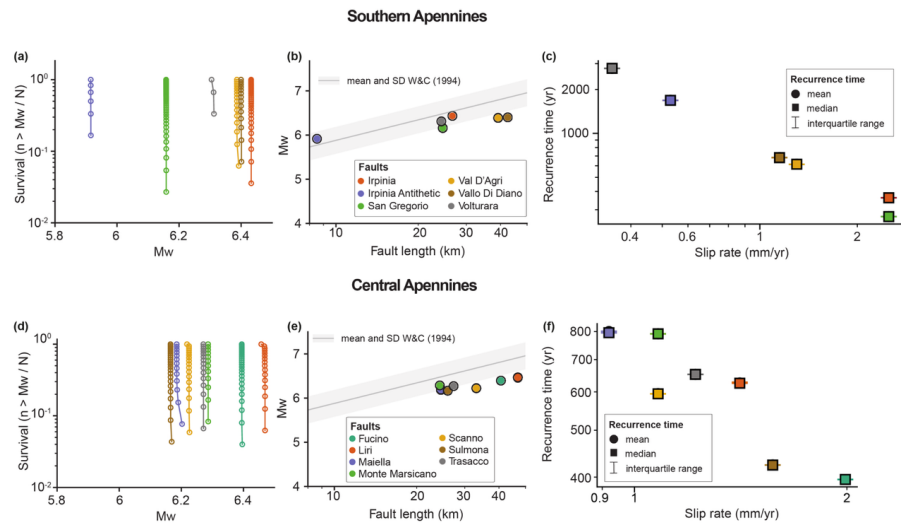
230

231 **4 Results**

232 **4.1 Seismic cycles on isolated faults**

233 In all single-fault simulations, faults rupture with a characteristic magnitude M_w (Fig. 3a,d), which is linearly
234 related to the logarithm of fault length (Fig. 3b,e). In the Southern Apennines, M_w on individual faults ranges
235 from 5.9 for the Irpinia Antithetic fault to 6.4 for the Irpinia and Vallo di Diano faults (Fig. 3a). In the Central
236 Apennines, M_w values range from 6.2 on the Sulmona fault to 6.5 on the Liri fault (Fig. 3d). Notably, most
237 earthquakes in both fault networks have magnitudes smaller than those predicted by empirical relationships of
238 subsurface rupture length vs. magnitude (Fig. 3b,e; Wells and Coppersmith, 1994).

239 The resulting seismic cycles are periodic, with recurrence intervals inversely correlated to the prescribed long-
240 term slip rate (Fig. 3c,f). Mean recurrence times range from 300 years in San Gregorio fault to ~1700 years in
241 Volturara fault in the Southern Apennines (Fig. 3c); and from 400 years in Fucino fault to 800 years in Maiella
242 fault in the Central Apennines (Fig. 3f).



243

244 **Figure 3: Earthquake cycle simulations of isolated faults in the (a-c) Southern and (d-f) Central Apennines.**
245 **(a, d) Magnitude-frequency distributions of earthquakes on each fault (shown as survival functions:**
246 **number of events with a Mw larger than a given value, normalised by the total number of events). Their**
247 **near vertical appearance indicates all isolated fault sin this model have characteristic-earthquake**
248 **behaviour, with very narrow range of Mw. (b, e) Comparison between modelled seismic events and mean**
249 **and standard deviation of empirical relationships of subsurface rupture length vs. Mw (Wells and**
250 **Coppersmith, 1994); (c, f) Mean, median and interquartile range of earthquake recurrence times vs. long-**
251 **term tectonic slip rate of individual faults. Note how the mean and median are equal, and the interquartile**
252 **range is below the marker size for all faults across both regions.**

253 **4.2. Seismic cycles on fault networks**

254 We generated two synthetic seismic catalogues for the interacting fault networks, containing 150 events in the
255 Southern Apennines and 154 events in Central Apennines (Fig. 4a,d). The magnitude range produced by faults
256 within the networks is broader than that of isolated faults: from Mw 5.3 to 6.8 in the Southern Apennines (Fig.
257 4c) and from Mw 5.3 to 7 in the Central Apennines (Fig. 4f), broadly matching observed earthquake magnitudes.
258 In our Southern Apennines model, the Alburni fault does not produce any earthquakes. This is likely due to its
259 shallow seismogenic zone (down to a depth of 2.65 km). Unlike the isolated fault models, not all ruptures extended
260 for the whole length of the faults, with some ruptures terminating as partial ruptures. Most faults generate both
261 full and partial ruptures, with a larger proportion of partial ruptures (Fig. 4b,e). Due to the generation of full and
262 partial ruptures, the magnitude-frequency distributions show a truncated Gutenberg-Richter distribution (Stirling
263 et al., 1996). The largest magnitude events are limited by the length of the longest fault, in our case, the Vallo di
264 Diano fault in Southern Apennines (Fig. 4c) and the Liri fault in Central Apennines (Fig. 4f). The Irpinia Antithetic
265 fault is the only fault to consistently generate full ruptures with a characteristic Mw of 5.8. This is likely due to



its small fault dimensions (8 km in length and depth), which limits its potential for partial ruptures in the model (Barbot, 2019; Cattania, 2019; Cattania and Segall, 2019) (Fig 4c,f).

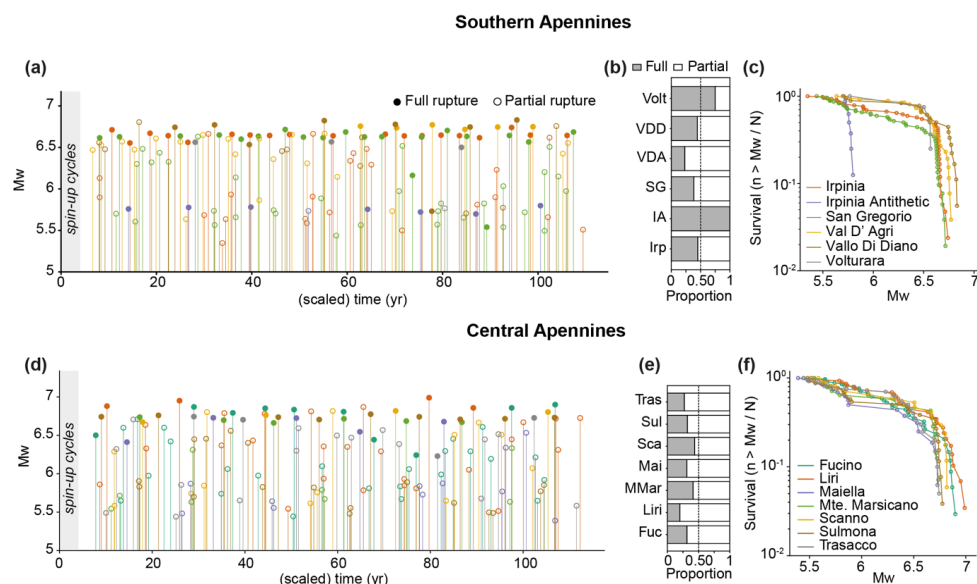


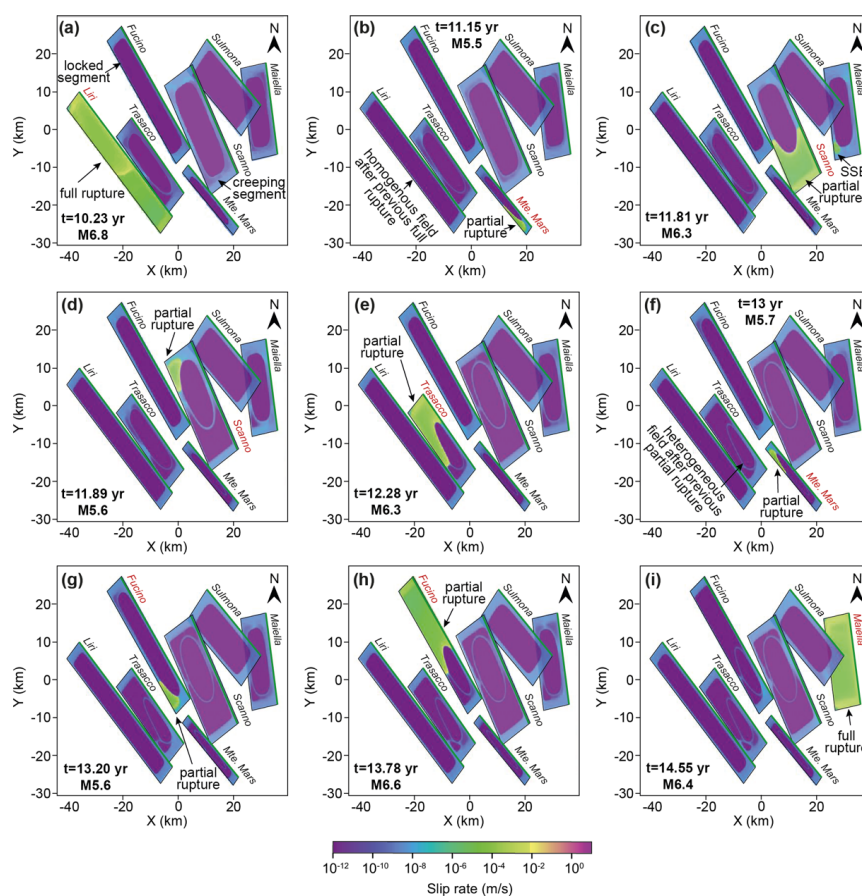
Figure 4: Earthquake statistics from the model results for the Southern (a-c) and Central (d-f) Apennines fault networks. Time distribution of simulated full- and partial-rupture events with stems and markers colour-coded by fault in the (a) Southern Apennines and (d) Central Apennines. Earthquakes in the first 5 yrs correspond to spin-up phases, thus are not included in the analysis. Given the use of a scaled slip rate, note that the simulated time (~110 yrs in both catalogues) is approximately equivalent to 11,000 yrs. (b, e) proportion of full and partial ruptures relative to the total number of events per fault in the (b) Southern Apennines and (e) Central Apennines. (c, f) Magnitude-frequency distributions of seismic events shown as survival function (number of events with a M_w larger than a given value normalised by total number of events) for each fault in (c) Southern Apennines and (f) Central Apennines. Colour legend for each fault is shown in panels (c) and (f).

279

To highlight the rupture styles observed in our simulation, Figure 5 shows a subset of events that occur in the Central Apennines between two full ruptures, one on the Liri fault and one on the Maiella fault. While a full rupture occurs on one fault, the remaining faults stay locked (Fig. 5a). The full rupture affects both the locked and surrounding creeping segment of the fault (Fig. 5a), and it is followed by partial ruptures in the remaining faults (Fig. 5b-h). Some of these partial ruptures occur consecutively on the same fault (e.g. Fucino fault, Fig. 5g-h), with some separated by tens of seconds (e.g. two events on the Vallo di Diano fault at 54.5 yr and two events on the Monte Marsicano fault at 83.6 yr, not shown in Fig. 5, Videos S2, S3; Rodriguez Picada et al., 2025c). Subsequent events in this type of sequence commonly rupture the fault segments that were not involved in the prior earthquake. Simulated full and partial ruptures nucleate typically at the base of the locked seismogenic zone



(Videos S2-S3, Rodriguez Picada et al., 2025c). Overall, while full-rupture events homogenise the slip rate field in locked fault patches (Fig. 5b), partial ruptures introduce a heterogeneous slip rate field in these patches (Fig. 5f), a direct consequence of the stress concentration left behind by the arrested partial ruptures. The heterogeneous slip rate then influences the nucleation and propagation of subsequent events (Video S2; Rodriguez Picada et al., 2025c), acting either as nucleation sites or barriers where ruptures terminate. In addition to the observed earthquakes, aseismic slip in the form of slow slip events sometimes occurs simultaneously with seismic events on other faults (Fig. 5c, Video S2, (Rodriguez Picada et al., 2025c). The occurrence of full and partial ruptures, as well as slow-slip events, shows the more diverse slip behaviour of faults within a network compared to the isolated fault models.



298

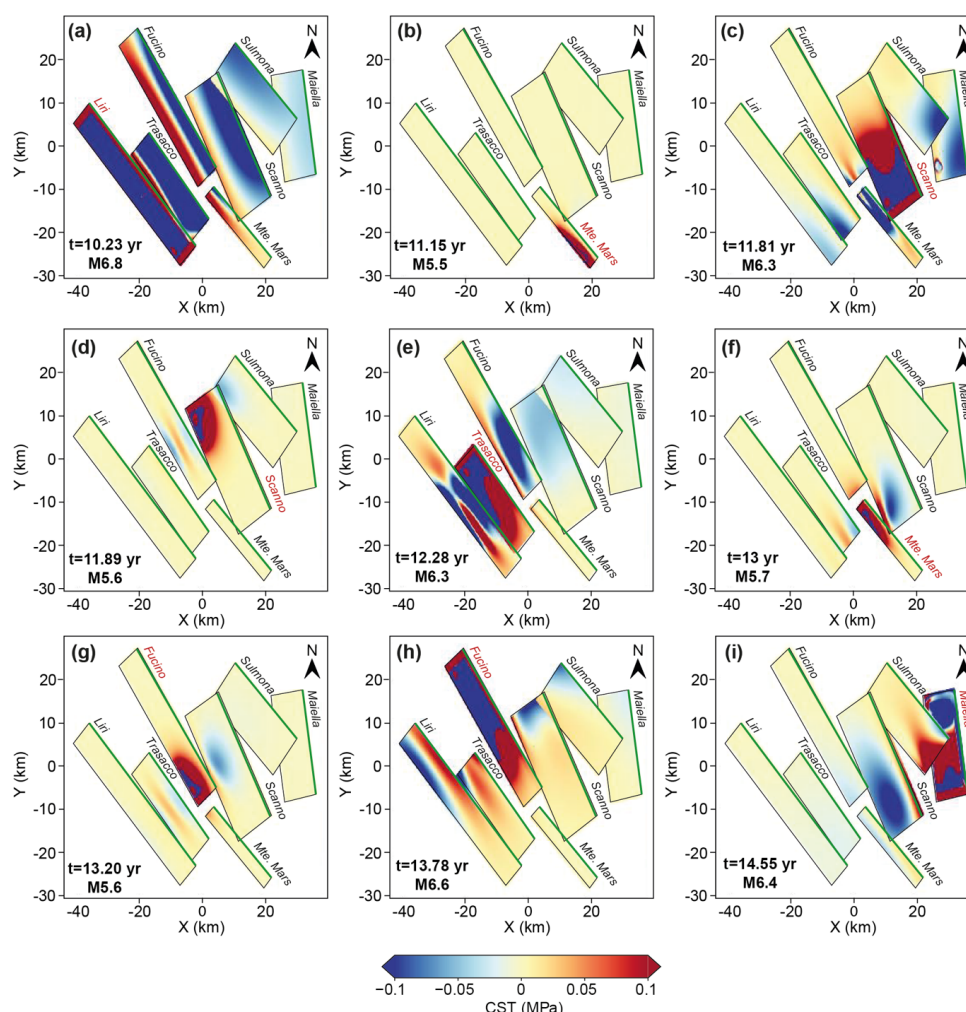
299 **Figure 5: Map view of slip-rate snapshots showing the final timestep of the coseismic phase for each event**
 300 **in a subset of modelled ruptures in the Central Apennines including full ruptures, partial ruptures and**
 301 **slow slip events (SSE). Monte Marsicano fault is abbreviated as Mte. Mars.**

302 To illustrate the stress changes introduced by each seismic event we computed the coseismic Coulomb stress
 303 transfer (CST) for each seismic event as (King et al., 1994):



$$\Delta C = \Delta \tau - \mu(\theta, V) \Delta \sigma \quad (5)$$

where $\Delta \tau$ is the shear stress-change, $\Delta \sigma$ is the normal stress change before and after the earthquake and $\mu(\theta, V)$ the rate-and-state friction coefficient at the receiver fault location. Figure 6 shows the CST for the same subset of modelled ruptures as in Fig. 5, and the CST evolution from all events in both fault network models are shown in Figs. S5 and S6. Most full and partial ruptures introduce a heterogeneous stress change on nearby faults, due to the range of fault strike and partial overlaps between faults in the network (Fig. 6). In the rare cases where faults are almost parallel and with a near 100% overlapping area, a full-rupture event on one fault introduces a homogenous stress change. This can be observed for the Liri and Trasacco faults, where a full-rupture event on Liri fault negatively loads Trasacco fault (Fig. 6a).



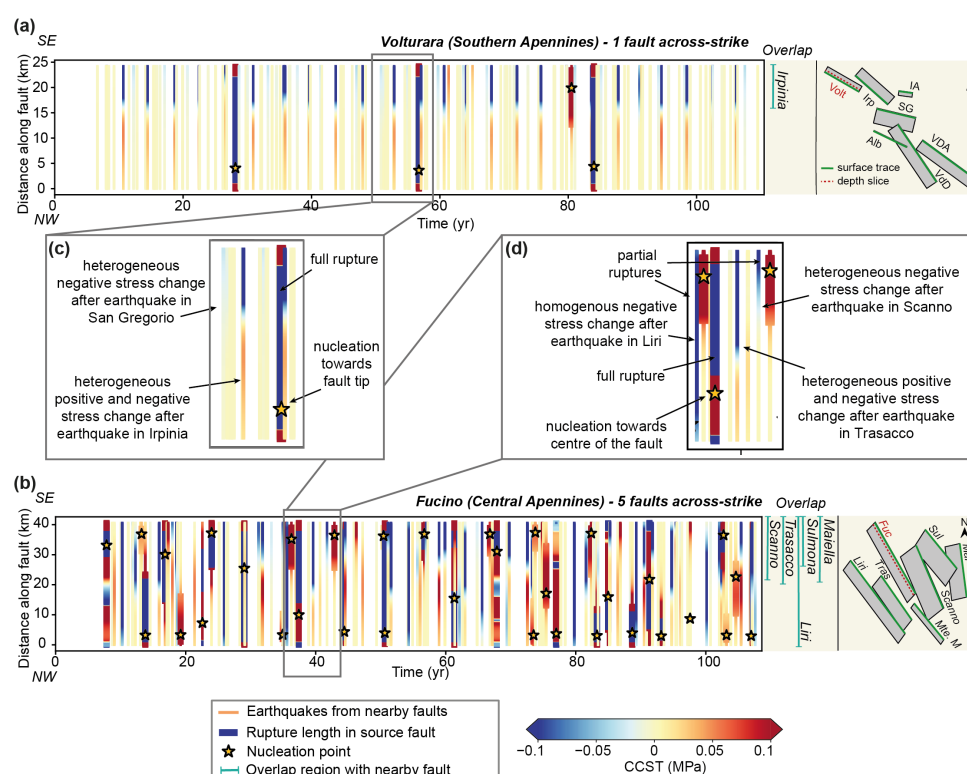
313

314 **Figure 6: Coseismic Coulomb Stress Transfer (CST) for a subset of modelled earthquakes in the Central**
315 **Apennines shown in Fig. 5, with fault planes projected to a horizontal surface.**



316

317 Figure 7a-b shows the evolution of CST and nucleation point of each event along a depth slice near the top of the
318 velocity-weakening asperities (~1700 m) of the Volturara and Fucino faults, compared to the extent of overlap
319 with adjacent faults in the fault network (Figures S7 and S8 show the same but for the remaining faults). Faults
320 with few partially overlapping across-strike nearby faults, such as Volturara, tend to show heterogeneous
321 coseismic stress changes from neighbouring faults and simple earthquake cycles comprising mainly full ruptures
322 that nucleate near fault tips (Fig. 7a, c). Conversely, faults with multiple neighbouring non-coplanar faults, such
323 as Fucino fault (Fig. 7b, d), show a more spatially heterogeneous stress evolution and complex earthquake cycles
324 consisting of full and partial ruptures. Additionally, the nucleation of full and partial ruptures is not necessarily
325 confined to fault tips. Instead, partial ruptures that are either isolated or the first in a sequence often occur in areas
326 where faults overlap. Therefore, the number and arrangement of across-strike faults, and the heterogeneous
327 coseismic stress changes they induce, have a strong control on the earthquake cycle of individual faults.



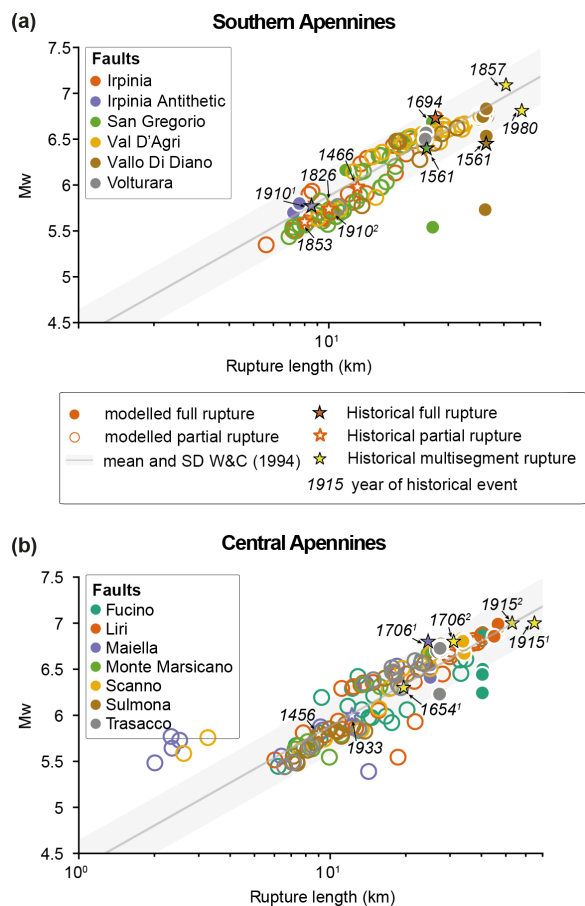
328

329 **Figure 7: (a) Coseismic Coulomb stress transfer (CST) on the Volturara fault, which has 1 across-strike**
330 **fault that overlaps; (b) CST on the Fucino fault, which has 5 neighbouring across-strike faults that overlap.**
331 **Coloured backgrounds show the stress changes following each event along a depth slice close to the top of**
332 **the velocity weakening asperity (location example shown in right panels of Fig. 7a,b). Coseismic CST due**
333 **to ruptures on the fault are indicated by the thick vertical slices that coincide with a star (nucleation point**



334 on the fault); thin vertical slices without corresponding star represent the coseismic CST due to ruptures
335 on neighbouring faults. On the right side of panels (a) and (b) we indicate the fault segments that are
336 overlapping with neighbouring faults (taken as the maximum length measured along-strike from the NW
337 fault tip, see Fig. D2, Appendix D), including an inset with map view of fault surfaces. (c) and (d) are zoom-
338 ins highlighting contrasting behaviours between the faults. The Volturara fault shows spatially
339 homogeneous stress changes and simple seismic cycles, with full ruptures and nucleation near fault tips.
340 The Fucino fault exhibits spatially complex coseismic CST patterns, partial ruptures, and nucleation that
341 is more distributed across the fault. Faults with limited across-strike interaction tend to show simpler
342 rupture behaviour, while those with multiple across-strike interactions show a more heterogeneous stress
343 evolution and complex earthquake cycle.

344 We compared the magnitudes and rupture lengths of the modelled events with historical seismicity (Table B1,
345 Appendix B) and empirical relationships between magnitude and subsurface rupture length (Wells and
346 Coppersmith, 1994); Fig. 8a-b). Our models are able to reproduce the magnitude and rupture length of the
347 historical single-fault events, including the two proposed scenarios for the 1910 earthquakes in Southern
348 Apennines (Galli and Peronace, 2014). However, we are unable to reproduce multi-fault events as recorded in the
349 historical seismicity catalogue (e.g. the 1857 and the 1980 seismic sequences in the Southern Apennines; one of
350 the proposed scenarios for the 1706 sequence and the 1915 sequence in the Central Apennines; Table B1,
351 Appendix B). Compared to the empirical relationships of magnitude vs. subsurface length, most of our modelled
352 events (99% in Southern Apennines and 92% in Central Apennines) fall within the range marked by the mean and
353 standard deviation of Wells & Coppersmith (1994).



354

355

356

357

358

359

360

361

362

363

364

365

366

367

368

Figure 8: Comparison between modelled seismic events, historical ruptures and empirical relationships of subsurface rupture length vs. M_w (Wells and Coppersmith; 1994) for (a) Southern Apennines and (b) Central Apennines. Modelled and historical single-fault events are colour-coded according to the source fault. Superindices on dates of historical events refer to alternative scenarios. 1910¹: scenario with rupture of entire Irpinia antithetic (Galli and Peronace, 2014); 1910²: scenario with 10-km rupture of Irpinia fault (Galli and Peronace, 2014); 1654¹: scenario with 13-km rupture of Southern section of Liri and entire Fibreno faults (outside of study area; (Guidoboni *et al.* 2019); 1706¹: scenario with rupture of entire Maiella fault (Guidoboni *et al.*, 2019); 1706²: scenario with rupture of entire Maiella and Palena faults (outside of study area; (Guidoboni *et al.*, 2019); 1915¹: scenario with rupture of entire Fucino, Parasano and San Sebastiano faults (Michetti *et al.*, 1996); 1915²: scenario with rupture of entire Fucino, Luco and Trasacco faults (Michetti *et al.*, 1996) (see Table B1, Appendix B).

366

367

368

Recurrence times vary between the two modelled regions, and depend on whether the full catalogue is considered, or whether it is split between full and partial ruptures. Full catalogue recurrence times for the system and for



individual faults are positively skewed, with some faults showing bi-modal distributions (Fig. 9). When the Southern and Central Apennines are compared, greater variability is observed in the mean recurrence times of the Southern Apennines, which range from 250 (San Gregorio fault) to 2100 (Vulturara fault) years in the Southern Apennines compared to 300 (Fucino fault) and 700 (Monte Marsicano fault) years in the Central Apennines (Fig. 9).

Where full and partial rupture catalogues are compared, partial ruptures tend to have shorter recurrence times than full ruptures (Fig 9a-b). Across both regions, recurrence time distributions of partial ruptures in individual faults and the system are positively skewed, spanning a wide range, from seconds to years. In contrast, the recurrence time distributions of full ruptures are narrower, typically following a bimodal or normal distribution (Fig 9).

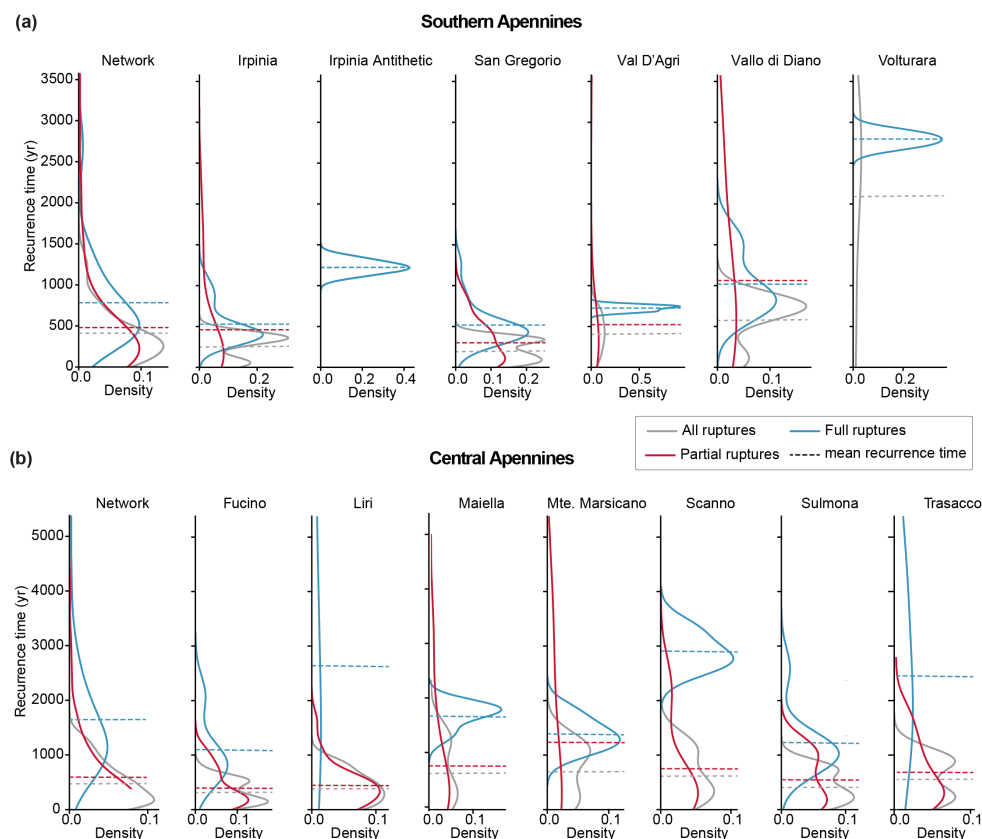


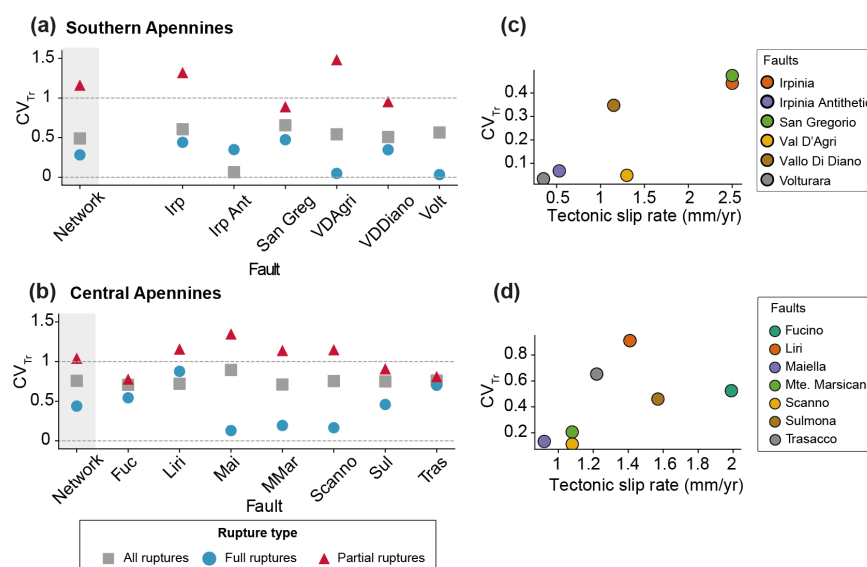
Figure 9: Variation of recurrence time (T_r) for the (a) Southern and (b) Central Apennines, shown as kernel density plots (KDE) and mean recurrence time, for the entire fault network and for individual faults considering the ‘All-ruptures’, ‘Full-ruptures’ and ‘Partial-ruptures’ catalogues. Vulturara fault produced only 1 partial rupture, thus no KDE for its partial-rupture catalogue could be computed. As this single partial rupture is included in the ‘All-ruptures’ catalog but absent from the ‘Full-rupture’ catalog, the two distributions are different. Note how the density scale varies by fault, and that partial ruptures typically display a greater range in recurrence time than full ruptures.



The catalogue periodicity is assessed through the coefficient of variation of recurrence time CV_{Tr} . For the all-rupture catalogues, both regions display weakly periodic behaviour ($CV_{Tr}=0.5-1$, Fig. 10a-b). The exception is the Irpinia Antithetic fault, which maintains a more periodic recurrence (Fig. 10a). Overall, the Central Apennines exhibits less periodic seismic cycles ($CV_{Tr}=0.8$, Fig. 10b) compared to the Southern Apennines ($CV_{Tr}=0.5$, Fig. 10a).

Periodicity differs between full and partial ruptures as well as between regions. Faults generate full rupture events with varying degrees of periodicity. In the Southern Apennines (Fig. 10a), all faults show strongly periodic full-rupture cycles ($CV_{Tr}<0.5$). In the Central Apennines (Fig. 10b), the behaviour is more variable: the Maiella, Monte Marsicano and Scanno faults show strongly periodic full-rupture cycles whereas the Trasacco, Liri, Sulmona and Fucino faults are weakly periodic ($0.5\leq CV_{Tr}<1$). Partial ruptures in both networks show less periodic behaviour than full ruptures (Fig. 10a-b). Their recurrence ranges from weakly periodic ($0.5\leq CV_{Tr}<1$; e.g., San Gregorio, Fucino, Sulmona and Trasacco faults) to random ($CV_{Tr}=1$, e.g., Vallo di Diano fault) or clustered ($1<CV_{Tr}<1.5$, e.g., Irpinia, Val D'Agri, Liri, Maiella, Monte Marsicano and Scanno faults). CV_{Tr} of full-rupture events tends to increase with increasing long-term slip rate (Fig. 10c-d).

400



401

Figure 10: (a-b) Coefficient of variation of recurrence times CV_{Tr} of seismic events (all events, full ruptures and partial ruptures) for individual faults and entire fault network in the (a) Southern Apennines and (b) Central Apennines. Horizontal dashed lines mark the CV_{Tr} values of perfectly periodic ($CV_{Tr}=0$) and lower limit of random ($CV_{Tr}=1$) seismic cycles. (c-d) Long-term slip rate vs. CV_{Tr} of all events for the (c) Southern Apennines and the (d) Central Apennines. Seismic cycles of full-rupture events are either strongly or weakly periodic, while cycles of partial ruptures are weakly periodic, random or clustered. The fault network in the Central Apennines has less periodic seismic cycles than in the Southern Apennines.



4.3 Relationships between seismic cycle characteristics and fault network geometry

In the Southern Apennines, where the fault network has fewer across-strike faults and larger distances between them, the across-strike interaction index (AI) is less than in the Central Apennines, which has multiple closely-spaced across-strike faults, resulting in a higher AI due to both fault number and proximity. Fault interactions via stress transfer affect recurrence intervals and magnitudes of full-rupture events, compared to the isolated fault case (Fig. 11). Most faults produce full ruptures with longer recurrence times and larger magnitudes compared to the reference cycles on isolated fault (Fig. 11). These differences become more pronounced with an increase in the number of nearby across-strike faults in the Central Apennines, as opposed to the Southern Apennines.

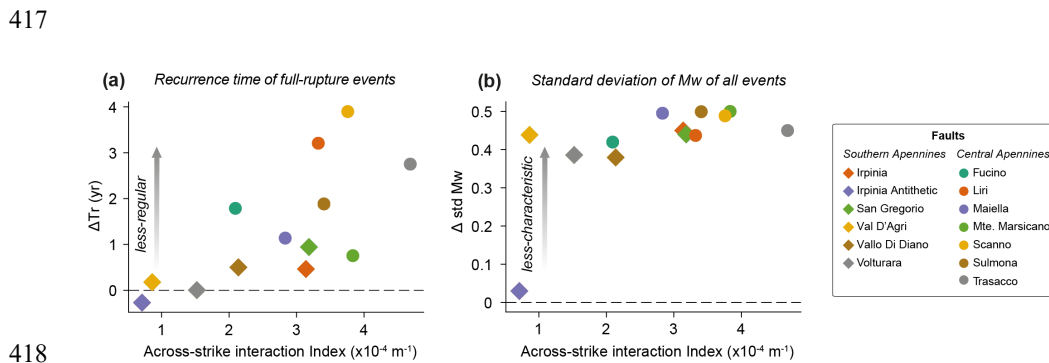
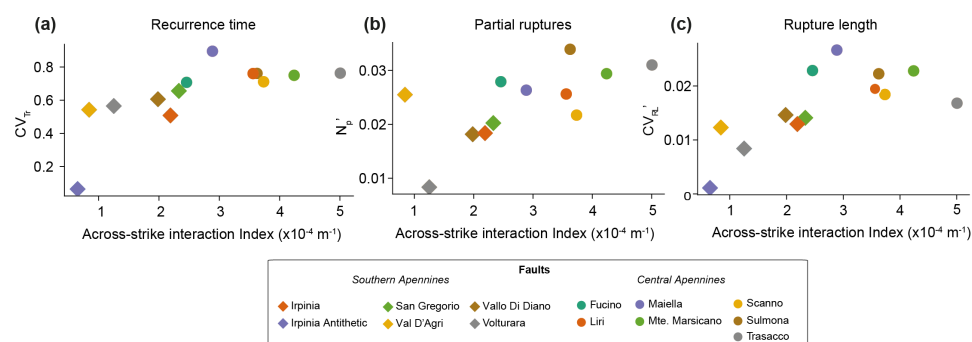


Figure 11: Comparison of earthquake cycles between single-fault simulations and fault-network simulations in terms of event (a) recurrence time (Tr) of full-rupture events ($\Delta Tr = \frac{mean Tr_{network} - mean Tr_{single}}{mean Tr_{single}}$) and (b) standard deviation of magnitude of full-rupture events $\Delta std Mw = \frac{std Mw_{network} - std Mw_{single}}{std Mw_{single}}$ as a function of the across-strike interaction index (eq. 1). $\Delta Tr=0$ indicates regular recurrence, while positive (negative) values correspond to longer (shorter) recurrence times in the fault-network simulations relative to the single-fault simulations. $\Delta std Mw=0$ indicates characteristic magnitude distribution, while increasingly positive values indicate broader magnitude-frequency distributions in the fault-network simulations. Faults with multiple faults across-strike (larger AI) show larger differences in recurrence time and standard deviations of magnitude compared to single-fault simulations, indicating a greater deviation from their characteristic periodic behaviour.

Differences in earthquake cycle properties between the Southern and Central Apennines are influenced by fault network geometry (Fig. 12). When considering both networks together, we observe consistent positive correlations between the across-strike interaction index GI and the three metrics of seismic complexity (CV_{Tr} , N_p' , and CV_{RL}') with mean Spearman values ranging from 0.46 to 0.84 (Table F1, Appendix F). When analysed separately, the Southern Apennines show strong correlations for CV_{Tr} and CV_{RL}' at some depths (Table F1), but no consistent trend for N_p' . In contrast the Southern Apennines show weak or no correlations for all metrics (Table F1). This suggest that the geometric effects become clearer when sampling a broader range of network configurations across both regions.



438



439

440 **Figure 12: Relationships between fault network geometry, described by the across-strike interaction index**
 441 **(AI), and (a) coefficient of variation of recurrence times (CV_{Tr}), (b) number of partial ruptures (N_p') and**
 442 **coefficient of variation of rupture lengths (CV_{RL}') for faults in the Southern and Central Apennines. AI is**
 443 **calculated at a depth of 7.5 km, approximately the middle fault depth. Plots corresponding to depths of 0**
 444 **km and 15 km are shown in Fig. F1 (Appendix F).**

445

446 5 Discussion

447 5.1 Comparison between simulated and natural seismic cycles in Italy

448 Italy's exceptional historical and paleoseismic record (D'Addezio et al., 1991; Galadini and Galli, 1996, 1999;
 449 Galli et al., 2006, 2008, 2016, 2014; Galli and Peronace, 2014; Pace et al., 2020; Pantosti et al., 1993) provides a
 450 valuable basis for evaluating our models. Our simulations are, to our knowledge, the first 3D continuum
 451 earthquake cycle models to combine rate-and-state friction with fault interactions across more than three faults,
 452 resolving nucleation and rupture self-consistently.

453 To compare with natural data, we focused on $M \geq 6.5$ events and recurrence intervals from paleoseismic trenching
 454 (Table B2; Pace et al., 2016). After scaling due the high slip rates used in our models, natural recurrence intervals
 455 are 1.3-9.4x longer than simulated ones, consistent with our use of maximum along-strike long-term slip rates,
 456 which likely overestimate loading and shorten cycles. We expect that incorporating realistic tapered profiles
 457 would bring simulated intervals closer to observations (Delogkos et al., 2023; Faure Walker et al., 2019).

458 Paleoseismic recurrence times show greater variability than our nearly periodic modelled seismic cycles for full
 459 ruptures. This may reflect incomplete long-term records (e.g., Lombardi et al., 2025; Mouslopoulou et al., 2025),
 460 temporal changes in slip rates documented by cosmogenic dating (Benedetti et al., 2013; Cowie et al., 2017;
 461 Mildon et al., 2022; Roberts et al., 2024, 2025; Sgambato et al., 2025), the greater geometrical complexity of
 462 natural faults, and possibly also a larger ratio W_s/L_∞ (Barbot, 2019; Cattania, 2019), all of which could enhance
 463 stress heterogeneity and variability.



464 While our models reproduce the magnitude range of historical single-fault events, they do not produce multi-fault
465 ruptures as documented in the historical catalogue in the region (Benedetti et al., 1998; Cello et al., 2003; Galli et
466 al., 2006). This likely stems from the quasidynamic approximation, which limits stress drops, slip velocities and
467 rupture jumping (Thomas et al., 2014). Using simulated cycles as initial conditions for fully dynamic rupture
468 models could help address this (Galvez et al., 2020).

469 Despite these limitations, our results show that SEAS models can capture key behaviours of complex fault
470 networks and generate synthetic earthquake catalogues that are directly comparable with paleoseismic data. This
471 provides a strong basis for future simulations integrating more geologically realistic features, such as along-strike
472 variations of slip rate and strike.

473 **5.2 Effect of stress redistribution within a fault network on simulated seismic sequences**

474 Our simulations show that earthquakes on networks with multiple across-strike faults, such as those in the Central
475 Apennines, generate spatially heterogeneous stress perturbations on nearby faults. These interactions promote
476 more partial ruptures, greater variability in rupture lengths and magnitude, and less periodic behaviour of large
477 earthquakes. In contrast, faults within more along-strike networks, like in the Southern Apennines, experience
478 more uniform stress loading and tend to produce more periodic and characteristic seismic cycles, behaviours more
479 similar to simulations of isolated faults (Figs. 4a, 12,13). These results build upon prior numerical modelling work
480 of (Rodriguez Piceda et al., 2025a), which showed that complex and non-periodic seismic cycles emerge in a
481 system of two across-strike normal faults. They also extend prior CST modelling work (Sgambato et al., 2020b,
482 2023), which showed that relatively isolated faults experience more regular stress loading histories dependent on
483 interseismic loading than networks with multiple faults arranged across-strike.

484 The effects of fault network geometry can be isolated when other factors such as long-term slip rate are considered
485 constant. A clear example of the influence of fault network geometry comes from the Central Apennines, where
486 the Scanno and Monte Marsicano faults have similar slip rates (Table 1), yet they have contrasting seismic cycle
487 characteristics. The Monte Marsicano fault exhibits more irregular rupture timing, partial ruptures and rupture
488 extent variability than the Scanno fault (Fig. 12), likely due to the influence of multiple closely-spaced CST
489 sources (Maiella, Sulmona, Scanno and Trasacco, Fig. E2e,f; E4, Appendix E), and therefore higher across-strike
490 interaction index.

491 Fault networks also show longer recurrence times and larger magnitudes of full-rupture events, than the same
492 faults modelled in isolation (Fig. 11). This results from stress interactions delaying full ruptures, allowing more
493 time for fault healing and strength recovery, which leads to larger stress drops and higher seismic moments.
494 Consequently, the magnitude versus rupture length scaling for fault networks (Fig. 8) better matches natural
495 variability (Wells and Coppersmith, 1994), indicating that stress interaction among faults may contribute to the
496 scatter seen in empirical scaling relationships.

497 Our focus is on normal fault networks, thus a remaining question is whether the findings will be applicable to
498 strike-slip and thrust faults. We speculate that similar effects could occur in these settings, with the outcome
499 depending on the degree of development of the fault network. Fault networks in late stage of development tend to



500 evolve into more localized structures, reducing the fault overlap and the extent of interactions. In contrast,
501 interaction effects may be more pronounced in early-stage networks, where a higher number of closely spaced
502 overlapping faults are more common.

503 **5.3 Role of long-term slip rate in stress interaction effects**

504 When faults have few stress interactions with others, as in the Southern Apennines, their seismic cycle is primarily
505 controlled by their long-term slip rate, with faster moving-faults having shorter recurrence times than slower-
506 moving faults (Fig. G1, Appendix G).

507 In both Central and Southern Apennines, faults with higher long-term slip rates are more responsive to positive
508 stress perturbations from nearby faults. For a given across-strike interaction index, faster-loading faults show less
509 periodic recurrence of full ruptures and more variable rupture lengths (Fig. 12). Indeed, as these faults approach
510 failure more often, they are more likely to be triggered by even small CST perturbations from nearby faults (e.g.,
511 Sulmona, Liri and Trasacco faults in Central Apennines, Fig. 12). In contrast, slower-loading faults, such as the
512 Volturara fault in the Southern Apennines (Fig. 7a), accumulate stress more slowly, experience stronger healing
513 and show more regular recurrence.

514 This finding partially contrasts with results of elastic-brittle lattice models (e.g. Cowie et al., 2012), which
515 associate higher CV with slower long-term slip rates in faults with multiple across-strike interactions. In those
516 models the absence of time-dependent stress healing means that slower loading allows heterogeneity to
517 accumulate over longer timescales, increasing CV. In our rate-and-state friction models, by contrast, we isolate
518 loading-rate effects at a fixed network geometry and find that CV increases with higher slip rate, consistent with
519 reduced interseismic healing for the same time interval and higher sensitivity to small CST perturbations.
520 Although the long-term slip-rate trends differ, both approaches agree that more complex fault networks lead to
521 greater recurrence variability.

522 **5.4 Implications of fault network geometry on seismic hazard assessment**

523 The fact that fault network geometry influences variability in earthquake recurrence and magnitude within a fault
524 system challenges the common practice in time-dependent seismic hazard assessment (SHA) of applying a single
525 mean recurrence time and coefficient of variation across the entire network (e.g., Nishenko and Buland, 1987,
526 Ellsworth et al., 1999; Matthews et al., 2002). In systems with numerous across-strike faults and high long-term
527 slip rates, CV values can vary greatly between individual faults, suggesting that hazard models should use broader
528 recurrence and magnitude-frequency distributions to reflect more irregular earthquake behaviour. Probabilistic
529 SHA could further benefit from integrating network-derived metrics, such as the across-strike interaction index,
530 into logic tree weights to better capture the seismic cycle complexity. In addition, time-dependent SHA models
531 based on CST history (Chan et al., 2010; Iacoletti et al., 2021; Mignan et al., 2018; Stein et al., 1997; Toda et al.,
532 1998) should also account for spatial variability in stress changes, which can affect the earthquake recurrence, a
533 limitation increasingly addressed by physics-based earthquake simulators (Milner et al., 2021; Shaw et al., 2018,
534 2022). Finally, our simulations indicate that overlap zones between faults can act as preferred nucleation sites and



constrain rupture extent (Fig. 7), highlighting their importance for assessing rupture scenarios and directivity effects (Spagnuolo et al., 2012; Thompson and Worden, 2017).

Overall, our study highlights how, by carefully considering the limitations, meaningful earthquake cycle statistics and the evolution of stress can be explored using SEAS simulations across complex fault networks, providing useful inputs into seismic hazard assessments of actively extending regions like Italy.

540

541 **6 Conclusions**

We numerically simulated seismic cycles on two fault networks in the Southern and Central Apennines to examine how changes in stress interactions caused by fault network geometry influence earthquake recurrence rates and magnitudes. Increased number of fault interactions leads to a greater departure from the characteristic and periodic behaviour of an isolated fault, with higher variability of earthquake recurrence, nucleation location and magnitude with increasing fault interaction. Fault networks with multiple across-strike faults are characterised by more complex seismic cycles than networks with fewer across-strike faults. When the number of across-strike interactions is similar, faults with higher slip rates tend to produce less-periodic earthquakes with more variable magnitude, meaning that slip rate influences how faults respond to stress changes from nearby ruptures. Our models demonstrate that, by carefully considering the numerical limitations, simulated earthquake catalogues can be meaningfully compared to natural earthquake records, highlighting the potential of using earthquake cycle modelling to assess the seismic hazard of complex normal fault networks.

553

554

555 **Appendix 1: SEAS governing equations and material properties**

Fault friction follows the rate-and-state friction law (Dieterich, 1979; Marone, 1998a; Ruina, 1983), where the shear stress (τ) along the fault is equal to its frictional strength:

$$558 \quad \tau = \mu\sigma(A1)$$

μ is the coefficient of friction and σ is the effective normal stress (total normal stress minus pore-fluid pressure). We adopt the regularised formulation of rate-and-state (Lapusta et al., 2000; Rice and Ben-Zion, 1996) where friction evolves with slip rate (V) and a state variable (θ) as:

$$562 \quad \mu(\theta, V) = a \sinh^{-1} \left[\frac{V}{2V^*} \exp \left(\frac{\mu^* + b \ln \left(\frac{V^* \theta}{D_c} \right)}{a} \right) \right] \quad (A2)$$

where μ^* is the reference coefficient of friction at a reference slip rate V^* ; a and b are constants for the magnitude of the contributions of the slip rate and fault state to the friction, respectively. D_c is the characteristic slip distance and it controls how the state variable evolves following the aging law (Dieterich, 1979; Ruina, 1983):



566
$$\frac{d\theta}{dt} = 1 - \frac{V\theta}{D_c} \quad (A3)$$

567 At steady state, $\frac{d\theta}{dt} = 0$, so steady state-friction is:

568
$$\mu_{ss} = a \sinh^{-1} \left[\frac{V}{2V^*} \exp \left(\frac{\mu^* + b \ln(\frac{V}{V^*})}{a} \right) \right] \quad (A4)$$

569 In this state, the parameter $(a - b)$ describes the dependence of μ_{ss} with velocity, with positive $(a - b)$
570 characteristic of velocity-strengthening materials (i.e. steady-state friction increases with increasing velocity) and
571 negative $(a - b)$ characteristic of velocity-weakening materials (i.e. steady-state friction decreases with
572 increasing velocity). Velocity-weakening materials can develop stick-slip behaviour, thus they are assumed to be
573 characteristic of the seismogenic portion of a fault or seismic asperity. To produce unstable sliding, the smallest
574 dimension (length L or width W) of a segment with velocity strengthening material must exceed a so-called
575 nucleation length (L_∞) (Rubin and Ampuero, 2005):

576
$$L_\infty = \frac{1}{\pi} \left(\frac{b}{b - a} \right)^2 \frac{G D_c}{b \sigma} \quad (A5)$$

577 where G is the shear modulus of the host rock. If the size of the velocity-weakening fault does not exceed the
578 nucleation length, aseismic slip will occur (Rubin and Ampuero, 2005).

579 To compute earthquake cycles, QDYN solves the equation of elasto-static equilibrium, where stress and slip rate
580 V are related by (Rice, 1993):

581
$$\tau_0 + \tau_e - \frac{G}{2c} V = \sigma \mu \quad (A6)$$

582 where τ_0 is the background shear stress, τ_e is the elastic shear stress due to fault slip, $\frac{G}{2c}$ is the radiation damping
583 term which approximates the inertial effects of seismic waves, c is the shear-wave speed, σ is the effective normal
584 stress, calculated by summing the initial normal stress σ_0 and the elastic normal stress σ_e from stress interactions:

585
$$\sigma = \sigma_0 + \sigma_e \quad (A7)$$

586 QDYN utilises the back-slip approach, such that the stresses transmitted from a fault element to neighbouring
587 elements are proportional to their slip deficit relative to the long-term tectonic slip (Heimisson, 2020; Savage,
588 1983). In this interpretation of backslip, faults are approximately modelled as faults of finite size loaded remotely
589 by tectonic stresses (Allam et al., 2019; Dieterich and Smith, 2010). When faults are remotely loaded in an elastic
590 medium, they tend to accumulate stresses indefinitely with increasing slip; however, due to the crust finite
591 strength, there should be some process of off-fault inelastic deformation to relax these stresses. The backslip
592 method approximately accounts for these inelastic processes, such that it maintains kinematic consistence with
593 the long-term slip rate of faults (Allam et al., 2019; Dieterich and Smith, 2010). The backslip approach
594 implemented in QDYN is the same as in Heimisson (2020).



595 The elastic shear stress at the i -th fault element τ_i^e due to the slip on the remaining fault elements is:

596
$$\tau_i^e = - \sum_j k_{ij}^{\tau} (u_j(t) - V_{PL} t) \quad (A8)$$

597 where V_{PL} is the long-term tectonic slip rate on the fault, u_j is the slip on the j -th cell and k_{ij}^{τ} is the stiffness matrix
598 for shear stress, which describes the shear stress change on the i -th fault element exerted by a unit slip on the j -th
599 fault element. The elastic normal stress σ_e from Eq. A7 is calculated similarly than in Eq. A8, but with the stiffness
600 matrix for normal stress k_{ij}^{σ} :

601
602
$$\sigma_i^e = - \sum_j k_{ij}^{\sigma} (u_j(t) - V_{PL} t) \quad (A9)$$

603 Both stiffness matrices in eqs. A8 and A9 are calculated using the analytical equations for static stresses induced
604 by rectangular dislocations in a homogeneous elastic half-space (Okada, 1992). Free surface conditions are
605 included in the formulations. Because the faults have varying orientations relative to one another, we are unable
606 to use optimizations that take advantage of the invariant strikes to construct the stiffness matrices, such as Fast
607 Fourier transforms (Rice, 1993). Instead, we use the implementation by Galvez et al., (2020) of the hierarchical
608 matrix (H-matrix) compression to the stress transfer component (Bradley, 2014) and the LSODA solver
609 implemented by Yin et al. (2023). Despite the improved time-stepping efficiency demonstrated in Yin et al.
610 (2023), the simulations remain computationally demanding, requiring approximately two months to complete.

611 The material and frictional properties are listed in Table A1. Each fault consists of a rectangular patch in the centre
612 with velocity-weakening properties, bounded by a velocity-strengthening region with a width of 1.5 km in the
613 Southern Apennines and 1.1 km in the Central Apennines. Additionally, a 1 km transition zone was set between
614 the velocity-strengthening and the velocity-weakening and regions.

615 The variation of normal stress with depth follows the approach by Lapusta et al. (2000), where effective normal
616 stress $\bar{\sigma}_l$ equals the lithostatic pressure minus the hydrostatic pore-fluid pressure at shallow depths, with a
617 transition to lithostatic pore pressure gradient with a 50 MPa offset at depth (z):

618
$$\bar{\sigma}_l = \min \left\{ \begin{array}{l} 2.8 + 18 * z / km \\ 50 MPa \end{array} \right. \quad (A10)$$

619 We account for the dip angle of the normal faults (α) in our simulations:

620
$$\bar{\sigma} = \bar{\sigma}_l \sin(\alpha) \quad (A11)$$

621 In this set up, where multiple faults are interacting, the normal stress can reach negative values near the surface.
622 To accommodate the possible stress change that could occur during the spin-up phase, the initial minimum normal
623 stress is increased to 15 MPa (Yin, 2022).



624

625 **Table A1:** Material and frictional properties of the model set up in the Central Apennines (CA) and Southern
626 Apennines (SA).

Symbol	Description (units)	Value
G	Shear modulus (GPa)	32
\square	Elastic modulus (GPa)	32
c	Shear wave velocity (m/s)	3000
μ^*	Reference friction coefficient	0.6
A	Direct-effect parameter	0.007
b	Evolution effect parameter	0.014 (VW) / 0.0042 (VS)
D_c	Characteristic slip distance (mm)	8 (SA), 10 (CA)
V_{PL}	loading rate	see table 1
V^*	Reference slip rate (m/s)	$=V_{PL}$
V_0	Initial slip rate (m/s)	0.8 V_{PL}
D_w, D_x	Cell size along-dip (m), Cell size along-strike (m)	110 (SA), 128 (CA)

627 **Appendix B: Historical and paleoseismicity of the Southern and Central Apennines**

628 **Table B1:** Historical seismic events (>0A.D.) based on (Mildon, 2017; Sgambato, 2022). *Magnitudes of
629 seismic events in Central Apennines prior to 1979 A.D. are taken from the Catalogue di Forti Terremoti
630 (Guidoboni et al., 2019) and are derived from the macroseismic shaking records (Gasperini and Ferrari,
631 2000) and as such are described as equivalent magnitudes (M_e , based on Mildon, 2017). For more recent



632 earthquakes in the Central Apennines post 1979 A.D. the magnitudes described are from seismological
 633 sources. ¹The name NW segment of Vallo di Diano often differs in the literature, being also known as
 634 Auletta fault or Caggiano fault (Bello et al., 2022; Galli et al., 2006)

Earthquake Date	Magnitude*	Source Fault	Proportion of the fault that slips	Reference
Southern Apennines				
15/01/1466	5.98	Irpinia	SE section 13 km	Marturano (2007)
31/07/1561	6.1	San Gregorio	Entire fault	Castelli et al. (2008)
19/08/1561	6.4-6.5	Vallo Di Diano ¹	all	Galli et al. (2006)
08/09/1694	6.73	Irpinia	All	Galli et al., (2006, 2014); Galli and Peronace (2014)
01/02/1826	5.74	Val d'Agri	Northern section 10 km	Rovida et al., (2020)
09/04/1853	5.6	Irpinia	Northern section 8 km	Galli and Peronace, (2014)
16/12/1857	7.12	Vallo di Diano and Val D'Agri	Northern section Vallo Di Diano (12km) + entire Val D'Agri	Benedetti et al., (1998); Cello et al. (2003); Galli et al. (2006)
07/06/1910	5.76	Irpinia Antithetic	Entire fault	Galli and Peronace (2014)
		Irpinia	Southern section of Irpinia (10 km)	
23/11/1980	6.81	Irpinia, San Gregorio? and Irpinia antithetic	Entire faults	Galli and Peronace (2014); Giardini et al. (1996); Rovida et al. (2020); Sgambato et al. (2025); Westaway, (1993); Westaway and Jackson (1987)
Central Apennines				



05/12/1456	5.8	Sulmona	Northern section (9km)	Guidoboni et al. (2019)
24/07/1654	6.3	Liri and Fibreno	Southern section of Liri (13 km) + entire Fibreno fault (6.6 km)	
3/11/1706	6.8	Maiella	Entire fault	Guidoboni et al. (2019)
		Maiella and Palena	Entire faults	
13/01/1915	7	Fucino, Parasano and San Sebastiano	Entire faults	Michetti et al. (1996)
		Fucino, Luco and Trassaco	Entire Fucino and Luco faults + northern section of Trasacco (8km)	
26/09/1933	6	Maiella	Central section (12.2 km)	Pizzi et al. (2010)

635

636 **Table B2: Paleoequakes and historical events in modelled faults of the Southern and Central**
637 **Apennines. The nomenclature of some of the faults adopted by Faure Walker et al. (2021) and Sgambato**
638 **et al. (2020) and in this study differs from that of the paleoseismic data: ¹part of the Monte Marzano fault**
639 **system by Galli (2020); ²part of this fault is the San Benedetto dei Marsi–Gioia dei Marsi segment in the**
640 **Fucino fault system in Galadini and Galli (1999); ³also known as Monte Morrone fault by Galli et al. (2015).**
641 **Paleoevents in bold are events with defined aged brackets used for the calculations of mean and standard**
642 **deviation of recurrence times in the Discussion section.**

Fault	N Paleoevents	Date of paleoevents	Reference
Southern Apennines			
Irpinia ¹	5	6736-8600 B.P.; 4411-6736 B.P; 3507-4283 B.P.; 1415-2754 B.P.; 1980 A.D. Pantano di San Gregorio Magno segment:	(D'Addezio et al., 1991; Pantosti et al., 1993)



		11,180–19,660 B.P., 6620–9420 B.P., 2570–6620 B.P., 1720–2570 B.P.; 1980 A.D	
Central Apennines			
Fucino-Ovindolli-Pezza ²	6	20,000–32,520 ± 500 B.P.; 12,729–7,576 B.P.; 3,500–3,300 B.P.; 426–782 AD; 1231 AD; 1915 AD	Galadini and Galli (1996, 1999); Galli et al. (2016)
Sulmona ³	6	Before 9,000 B.P.; 6,500–8,500 B.P.; 5,500 B.P.; 200 AD, 1456 AD	Galli et al. (2015)
Trasacco	7	After 12,600 B.P.; 12,600–12,000 B.P. ; 7,000–6,600B.P.; 6,500–5,900B.P.; 3,500–3,600 B.P. to 3,400–3,500 B.P.; 1,500– 1,600B.P. or 1,500–1,400 B.P.; 1915 AD	Galadini and Galli, (1999)
Liri	3	Before 12,500 B.P.; before 5,000 B.P.; before 1,500 B.P.	Pace et al., (2020)

Table B3: Comparison between recurrence times (mean and standard deviation in years) derived from historical and paleoseismological data (Tr_{paleo}) and modelled seismic events (Tr_{model}). Only paleoseismic events with well-defined age brackets were included in the calculation (see Table B2). Tr_{paleo} = recurrence times based on historical and paleoseismological data from the past 20 kyr. Scaled Tr_{model} = recurrence times from modeled seismic events adjusted by the correction factor.

Fault	$Tr_{paleo} \pm \sigma$	Scaled Tr_{model}
Irpinia (SA)	1900 ± 186	454±161
Fucino (CA)	4253 ± 4465	900±720
Sulmona (CA)	1866±1231	1440±620
Trasacco (CA)	2469±1259	1217±290

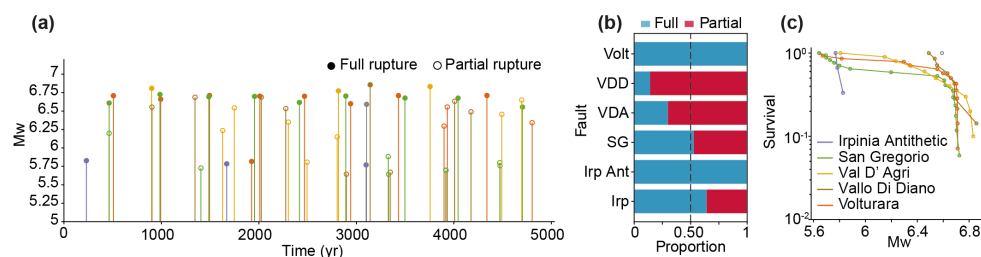


Figure C1: synthetic catalog for a simulation of the Southern Apennines with nominal values of prescribed long-term slip rate. (a) Time distribution of simulated full- and partial-rupture events with stems and markers color-coded by fault (b) (b,e) proportion of full and partial ruptures per fault. (c) Magnitude-frequency distributions of seismic events shown as survival function (number of events with a Mw larger than a given value normalized by total number of events) for each fault. Color legend for each fault is shown in panels (c).

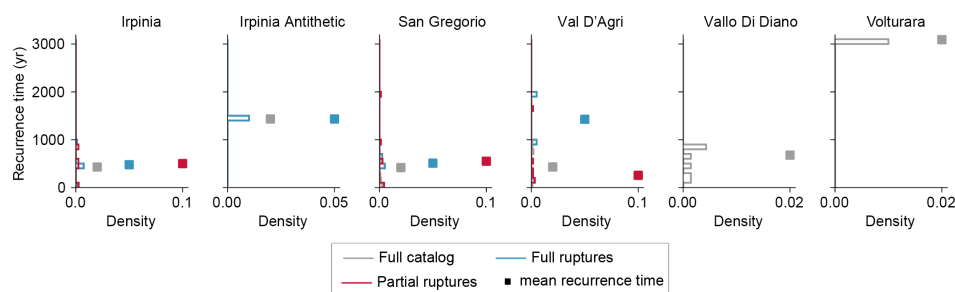


Figure C2: Variation of recurrence time of individual faults (step density histogram and mean recurrence time) and of the entire fault system for seismic events considering the full catalog, full-rupture and partial-rupture events of the fault networks for a simulation of the Southern Apennines with nominal values of prescribed long-term slip rate.

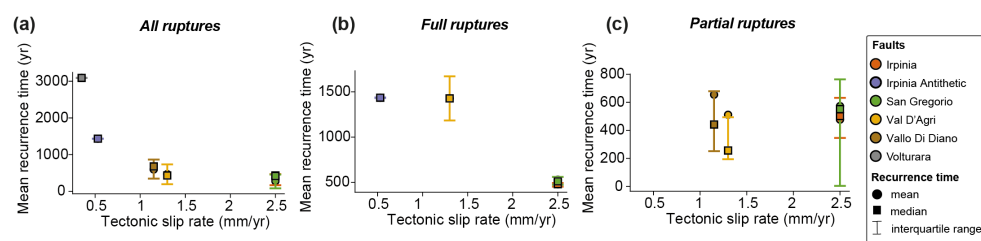
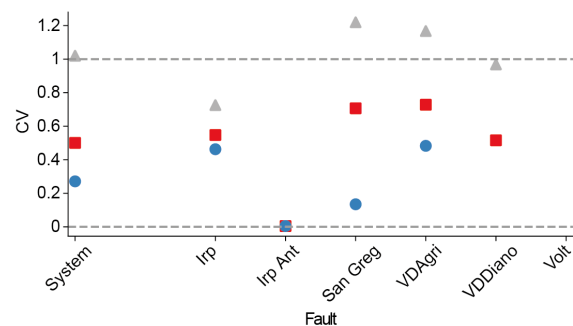


Figure C3: Mean, median and interquartile range of recurrence time of seismic events vs. (scaled) long-term tectonic slip rate of individual faults for a simulation of the Southern Apennines with nominal values of prescribed long-term slip rate.



668

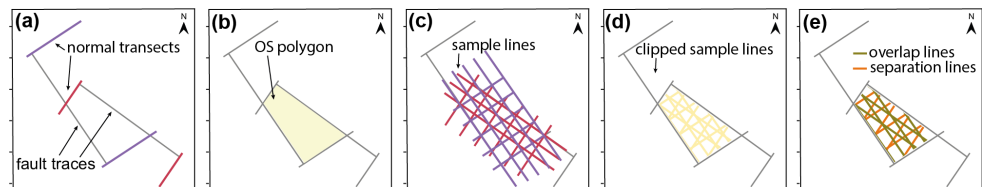
669 **Figure C4: Coefficient of variation of recurrence times CV_{Tr} of seismic events (all events, only full ruptures**
670 **and only partial ruptures) for individual faults and entire fault system for a simulation of the Southern**
671 **Apennines with nominal values of prescribed long-term slip rate.**

672

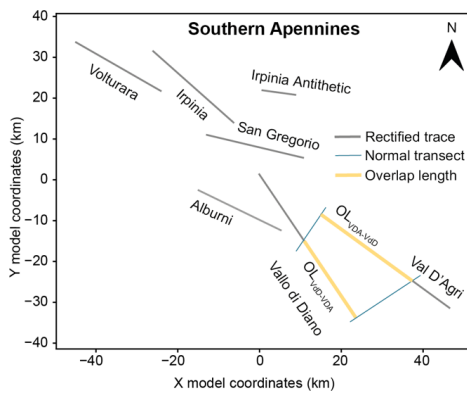
673 **Appendix D: Determination of separation between faults**

674 To determine the separation between two faults at depths of 0, 7.5 and 15 km we followed the following steps.
675 First, for all fault traces, we created bounding transects normal to the fault tips (Fig. D1a). Second, for each fault
676 pair, we drew a polygon bounded by two of the transects (one for each fault) and the fault traces (Fig. D1b). Third,
677 we created sample lines (separation lines) equally spaced by 100 m parallel to the transects (Fig. D1c). Lines that
678 did not intersect the fault traces or the transects were removed. Fourth, we clipped the sample lines to the polygon
679 area (Fig. D1d-e). Finally, for each set of overlap and separation lines, we computed the average length (preferred
680 value) and standard deviation. The workflow was carried out with QGIS (QGIS Development Team, 2009).

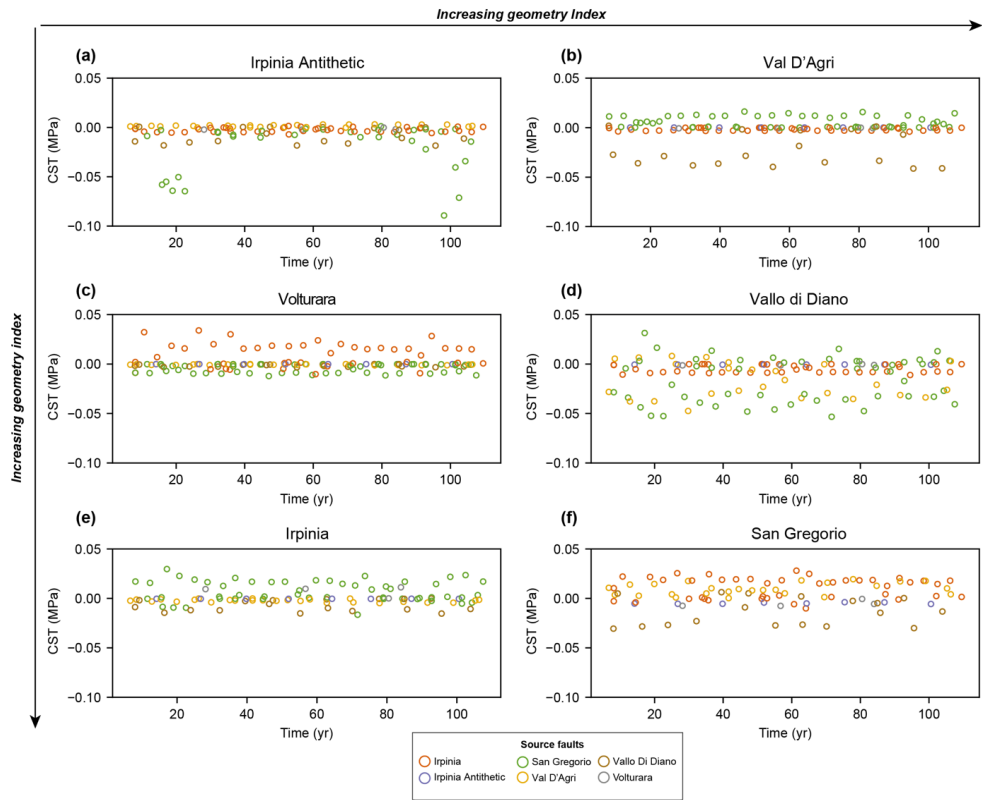
681



682 **Figure D1: illustrative workflow used to determine the separation between two fault traces at a given depth.**

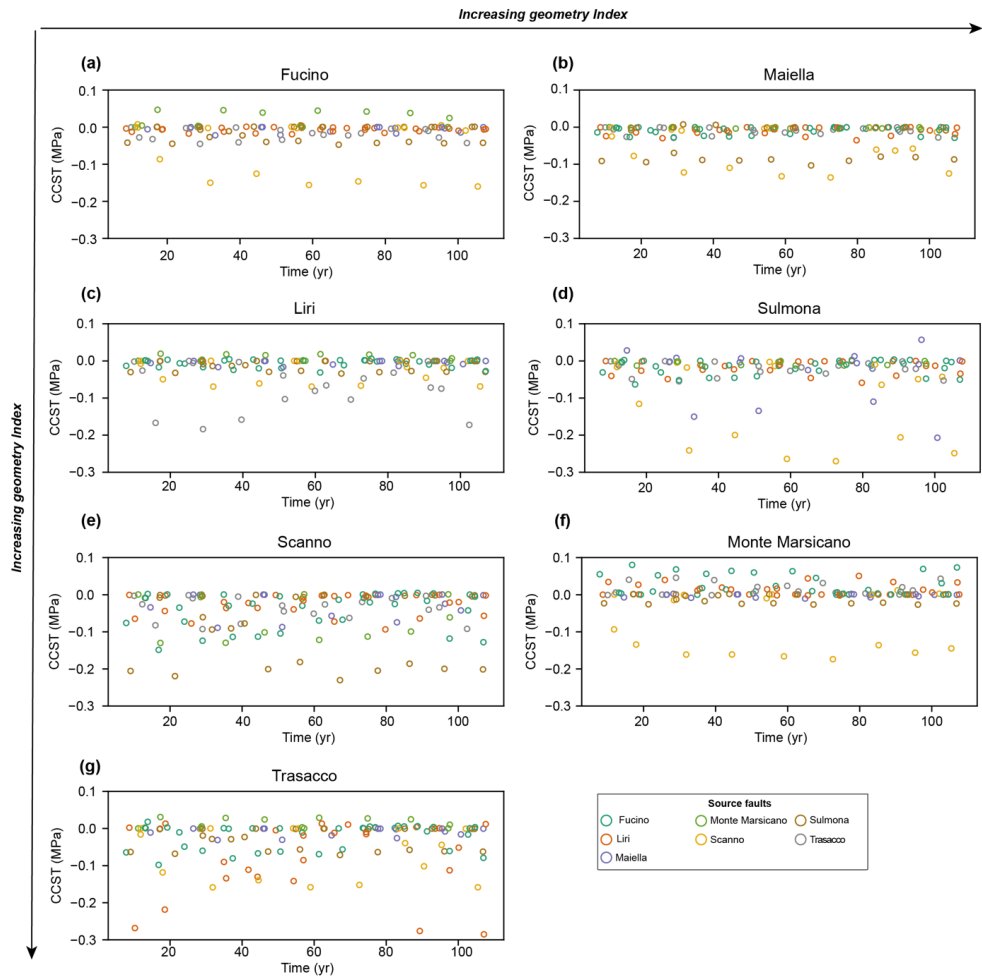


683
684 **Figure D2: Determination of overlap length between two faults (in this example, Vallo Di Diano and Val**
685 **D'Agri fault in the Southern Apennines) used for Figure 7 and S7-S8. To determine the overlap length**
686 **between two given faults (fault 1 and 2), we measure the distance along the strike of fault 1 between the**
687 **normal transect to one of the tips of fault 1 to the normal transect of to one of the tips of fault 2.**
688 **Appendix E: Coseismic coulomb stress transfer**

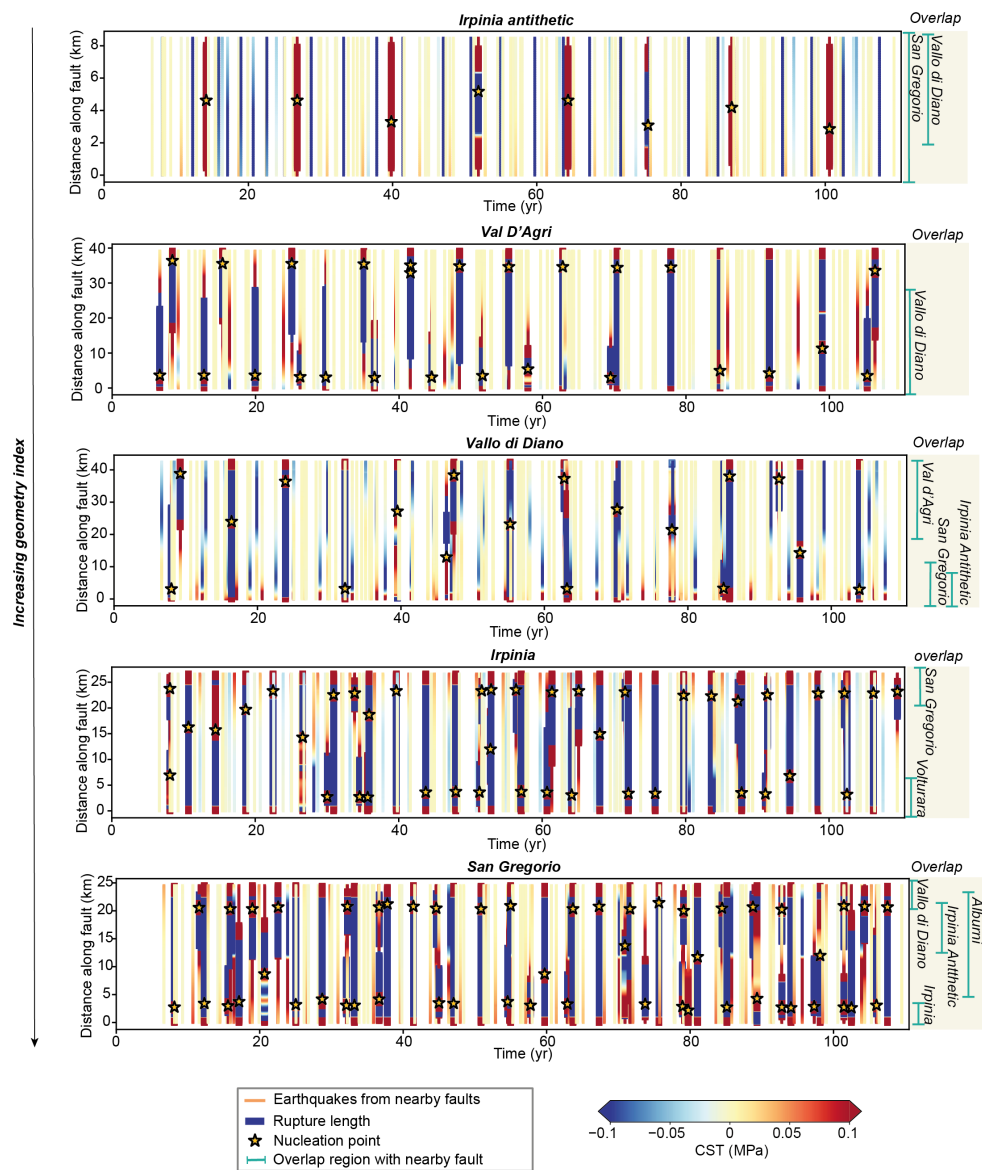




691 **Figure E1: Time series with coseismic Coulomb stress transfer (CST) averaged across the fault surface**
692 **induced by nearby faults in the Southern Apennines.**

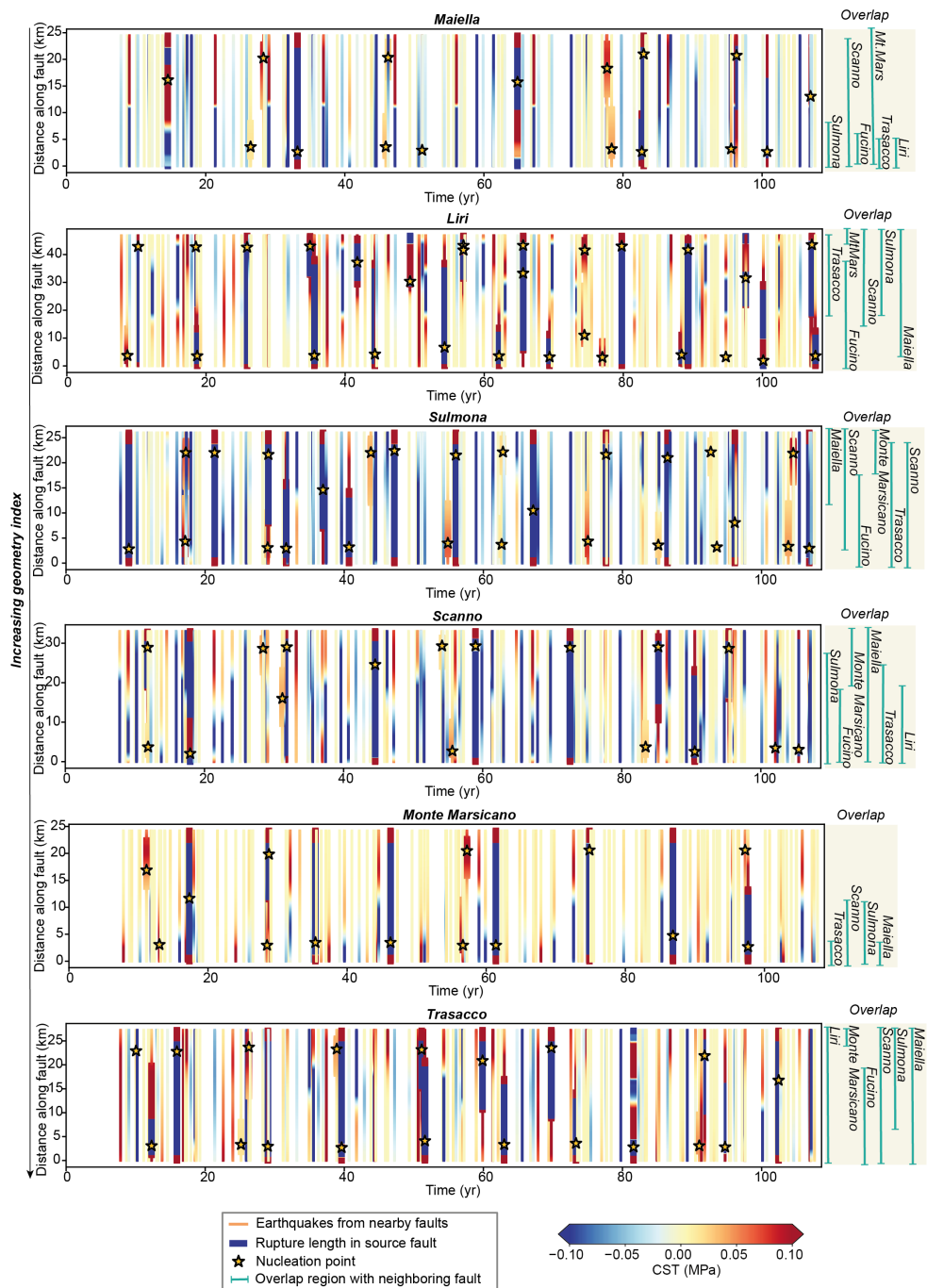


693
694
695 **Figure E2: Time series with coseismic stress transfer averaged across the fault surface induced by nearby**
696 **faults in the Central Apennines.**



697
698 **Figure E3: Coseismic stress transfer (CST) in the Irpinia Antithetic, Val D'Agri, Vallo di Diano, Irpinia**
699 **and San Gregorio faults in the southern Apennines. For the figure explanation, see caption of Figure 8 in**
700 **the main text.**

701
702
703
704



705

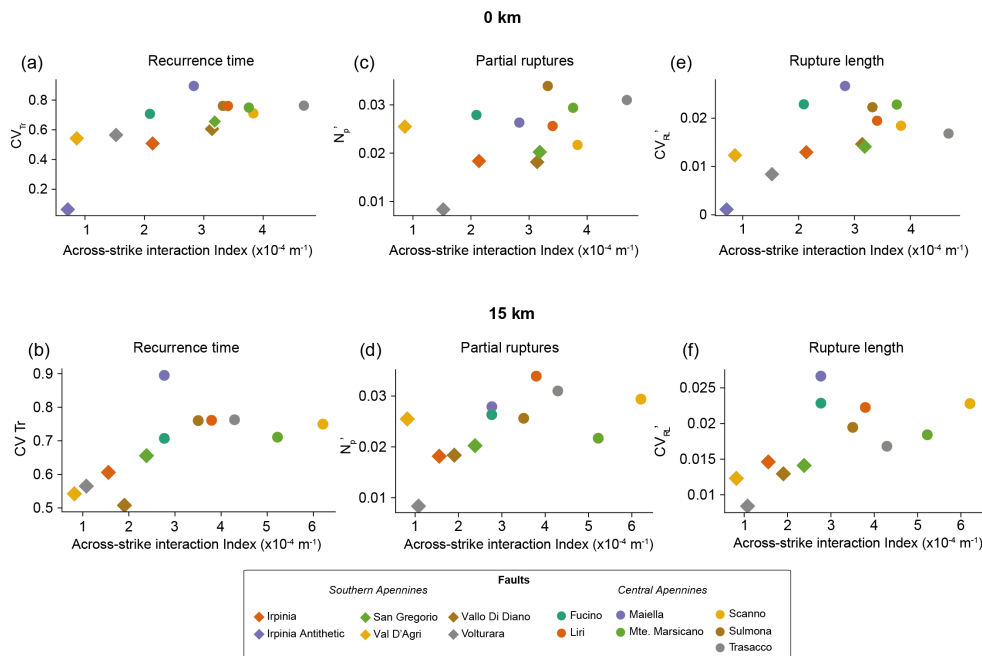
706



707 **Figure E4: Coseismic stress transfer (CST) in the Maiella, Liri, Sumona, Scanno, Monte Marsicano and**
708 **Trasacco faults in the Central Apennines. For the figure explanation, see caption of Figure 8 in the main**
709 **text.**

710

711 **Appendix F: Across-interaction index**



712

713 **Figure F1: relationships between fault network geometry, described by the across-strike interaction index**
714 **(AI), and (a-b) coefficient of variation of recurrence times (CV_{Tr}), (b-c) number of partial ruptures (N_p')**
715 **and (d-e) coefficient of variation of rupture lengths ($CV_{r'l}'$) for faults in the Southern and Central**
716 **Apennines. GI index corresponds to a depth of (a,d,e) 0 km and (b,d,f) 15 km.**

717

718 **Table F1: Leave-one-out Spearman's correlation coefficients (mean, standard deviation, minimum,**
719 **maximum) for relationship between across-strike interaction index (taken at 0 km, 7.5km and 15km) and**
720 **coefficient of variation of recurrence times (CV_{Tr}), number of partial ruptures (N_p') and coefficient of**
721 **variation of rupture lengths ($CV_{r'l}'$) for faults in the Southern and Central Apennines**

Depth (km)	metric	Mean ρ	Std ρ	Min ρ	Max ρ
Southern Apennines + Central Apennines					
0	CV_{Tr}	0.72	0.05	0.64	0.85
	N_p'	0.46	0.08	0.34	0.58



	CV_{rl}'	0.50	0.09	0.37	0.67
7.5	CV_{Tr}	0.84	0.03	0.80	0.90
	N_p'	0.73	0.05	0.68	0.85
	CV_{rl}'	0.71	0.06	0.64	0.78
15	CV_{Tr}	0.70	0.06	0.62	0.81
	N_p'	0.69	0.06	0.65	0.85
	CV_{rl}'	0.66	0.07	0.57	0.75
Southern Apennines only					
0	CV_{Tr}	0.82	0.13	0.70	1.00
	N_p'	-0.08	0.50	-0.40	0.80
	CV_{rl}'	0.87	0.05	0.80	0.90
7.5	CV_{Tr}	0.40	0.42	-0.20	1.00
	N_p'	0.04	0.54	-0.20	1.00
	CV_{rl}'	0.56	0.17	0.40	0.80
15	CV_{Tr}	0.65	0.23	0.40	1.00
	N_p'	0.04	0.54	-0.20	1.00
	CV_{rl}'	0.75	0.10	0.60	0.90
Central Apennines only					
0	CV_{Tr}	0.09	0.28	-0.43	0.43
	N_p'	0.00	0.24	-0.37	0.31
	CV_{rl}'	-0.84	0.06	-0.94	-0.77
7.5	CV_{Tr}	-0.27	0.25	-0.71	0.14
	N_p'	0.13	0.22	-0.09	0.60
	CV_{rl}'	-0.56	0.20	-0.89	-0.31
15	CV_{Tr}	0.18	0.27	-0.31	0.54
	N_p'	0.31	0.18	0.09	0.60



	CV_{rl}'	-0.70	0.12	-0.89	-0.54
--	------------	-------	------	-------	-------

Appendix G: Recurrence time and tectonic slip rate

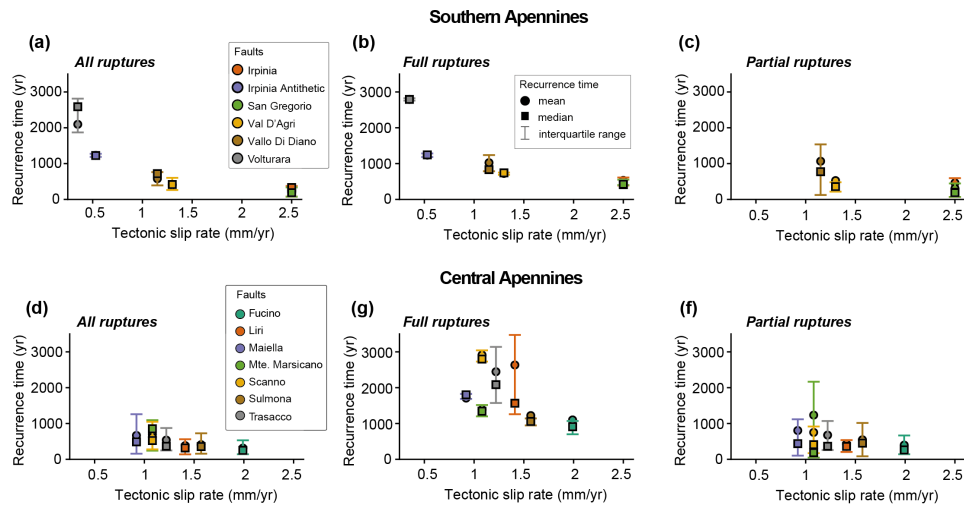


Figure G1: Mean, median and interquartile range of recurrence time of seismic events vs. long-term tectonic slip rate of individual faults for (a) Southern Apennines and (b) Central Apennines

Acknowledgements

This research was funded by UK Research and Innovation (UKRI) under the auspices of the project QUAKE4D (MR/T041994/1) awarded to Zoë Mildon. This work was carried out using the computational facilities of the ARCHER2 UK National Supercomputing Service (<https://www.archer2.ac.uk>). J.P.A. was supported by the French government through the UCAJEDI Investments in the Future project (ANR-15-IDEX-01) managed by the National Research Agency (ANR). Y.Y. was supported by the Swiss National Science Foundation Postdoc.mobility Grant P500PN_214179.

Code and data availability

Data to build the fault sources was taken from open-access publications (Faure Walker et al., 2019b; Mildon, 2017; Sgambato, 2022; Valentini et al., 2017). QDYN is open source (Luo et al. 2017). The modified code version used in this work can be found in (Rodriguez Piceda et al., 2025b). Input files to reproduce the results of this work are accessible in (Rodriguez Piceda et al., 2025c).



741 **Competing interests**

742 The authors declare no conflicts of interest.

743

744 **References**

745 Allam, A. A., Kroll, K. A., Milliner, C. W. D., and Richards-Dinger, K. B.: Effects of Fault
746 Roughness on Coseismic Slip and Earthquake Locations, *Journal of Geophysical Research:*
747 *Solid Earth*, 124, 11336–11349, <https://doi.org/10.1029/2018JB016216>, 2019.

748 Anderson, H. and Jackson, J.: Active tectonics of the Adriatic Region, *Geophysical Journal of*
749 *the Royal Astronomical Society*, 91, 937–983, [https://doi.org/10.1111/j.1365-](https://doi.org/10.1111/j.1365-246X.1987.tb01675.x)
750 [246X.1987.tb01675.x](https://doi.org/10.1111/j.1365-246X.1987.tb01675.x), 1987.

751 Bagh, S., Chiaraluce, L., De Gori, P., Moretti, M., Govoni, A., Chiarabba, C., Di Bartolomeo,
752 P., and Romanelli, M.: Background seismicity in the Central Apennines of Italy: The Abruzzo
753 region case study, *Tectonophysics*, 444, 80–92, <https://doi.org/10.1016/j.tecto.2007.08.009>,
754 2007.

755 Barbot, S.: Slow-slip, slow earthquakes, period-two cycles, full and partial ruptures, and
756 deterministic chaos in a single asperity fault, *Tectonophysics*, 768, 228171,
757 <https://doi.org/10.1016/j.tecto.2019.228171>, 2019.

758 Bello, S., Lavecchia, G., Andrenacci, C., Ercoli, M., Cirillo, D., Carboni, F., Barchi, M. R., and
759 Brozzetti, F.: Complex trans-ridge normal faults controlling large earthquakes, *Sci Rep*, 12,
760 10676, <https://doi.org/10.1038/s41598-022-14406-4>, 2022.

761 Benedetti, L., Tapponnier, P., King, G. c. p., and Piccardi, L.: Surface Rupture of the 1857
762 Southern Italian Earthquake?, *Terra Nova*, 10, 206–210, [https://doi.org/10.1046/j.1365-](https://doi.org/10.1046/j.1365-3121.1998.00189.x)
763 [3121.1998.00189.x](https://doi.org/10.1046/j.1365-3121.1998.00189.x), 1998.

764 Benedetti, L., Manighetti, I., Gaudemer, Y., Finkel, R., Malavieille, J., Pou, K., Arnold, M.,
765 Aumaître, G., Bourlès, D., and Keddadouche, K.: Earthquake synchrony and clustering on
766 Fucino faults (Central Italy) as revealed from in situ ³⁶Cl exposure dating, *Journal of*
767 *Geophysical Research: Solid Earth*, 118, 4948–4974, <https://doi.org/10.1002/jgrb.50299>, 2013.

768 Bernard, P. and Zollo, A.: The Irpinia (Italy) 1980 earthquake: Detailed analysis of a complex
769 normal faulting, *Journal of Geophysical Research: Solid Earth*, 94, 1631–1647,
770 <https://doi.org/10.1029/JB094iB02p01631>, 1989.

771 Boschi, E., Gasperini, P., and Mulargia, F.: Forecasting where larger crustal earthquakes are
772 likely to occur in Italy in the near future, *Bulletin of the Seismological Society of America*, 85,
773 1475–1482, <https://doi.org/10.1785/BSSA0850051475>, 1995.

774 Bradley, A. M.: Software for Efficient Static Dislocation–Traction Calculations in Fault
775 Simulators, *Seismological Research Letters*, 85, 1358–1365,
776 <https://doi.org/10.1785/0220140092>, 2014.



- 777 Cattania, C.: Complex Earthquake Sequences On Simple Faults, *Geophysical Research Letters*,
778 46, 10384–10393, <https://doi.org/10.1029/2019GL083628>, 2019.
- 779 Cattania, C. and Segall, P.: Crack Models of Repeating Earthquakes Predict Observed
780 Moment-Recurrence Scaling, *Journal of Geophysical Research: Solid Earth*, 124, 476–503,
781 <https://doi.org/10.1029/2018JB016056>, 2019.
- 782 Cavinato, G. P. and Celles, P. G. D.: Extensional basins in the tectonically bimodal central
783 Apennines fold-thrust belt, Italy: Response to corner flow above a subducting slab in retrograde
784 motion, *Geology*, 27, 955–958, [https://doi.org/10.1130/0091-7613\(1999\)027%253C0955:EBITB%253E2.3.CO;2](https://doi.org/10.1130/0091-7613(1999)027%253C0955:EBITB%253E2.3.CO;2), 1999.
- 786 Cello, G., Tondi, E., Micarelli, L., and Mattioni, L.: Active tectonics and earthquake sources
787 in the epicentral area of the 1857 Basilicata earthquake (southern Italy), *Journal of*
788 *Geodynamics*, 36, 37–50, [https://doi.org/10.1016/S0264-3707\(03\)00037-1](https://doi.org/10.1016/S0264-3707(03)00037-1), 2003.
- 789 Chan, C.-H., Sørensen, M. B., Stromeyer, D., Grünthal, G., Heidbach, O., Hakimhashemi, A.,
790 and Catalli, F.: Forecasting Italian seismicity through a spatio-temporal physical model:
791 importance of considering time-dependency and reliability of the forecast, *Annals of*
792 *Geophysics*, 53, 129–140, <https://doi.org/10.4401/ag-4761>, 2010.
- 793 Chiarabba, C., Jovane, L., and DiStefano, R.: A new view of Italian seismicity using 20 years
794 of instrumental recordings, *Tectonophysics*, 395, 251–268,
795 <https://doi.org/10.1016/j.tecto.2004.09.013>, 2005.
- 796 Chiaraluce, L., Barchi, M., Collettini, C., Mirabella, F., and Pucci, S.: Connecting seismically
797 active normal faults with Quaternary geological structures in a complex extensional
798 environment: The Colfiorito 1997 case history (northern Apennines, Italy), *Tectonics*, 24,
799 <https://doi.org/10.1029/2004TC001627>, 2005.
- 800 Chiaraluce, L., Michele, M., Waldhauser, F., Tan, Y. J., Herrmann, M., Spallarossa, D., Beroza,
801 G. C., Cattaneo, M., Chiarabba, C., De Gori, P., Di Stefano, R., Ellsworth, W., Main, I.,
802 Mancini, S., Margheriti, L., Marzocchi, W., Meier, M.-A., Scafidi, D., Schaff, D., and Segou,
803 M.: A comprehensive suite of earthquake catalogues for the 2016–2017 Central Italy seismic
804 sequence, *Sci Data*, 9, 710, <https://doi.org/10.1038/s41597-022-01827-z>, 2022.
- 805 Cinque, A., Ascione, A., and Caiazza, C.: Distribuzione spazio-temporale e caratterizzazione
806 della fagliazione quaternaria in Appennino meridionale., *ITA*, 2000.
- 807 Cowie, P. A., Roberts, G. P., Bull, J. M., and Visini, F.: Relationships between fault geometry,
808 slip rate variability and earthquake recurrence in extensional settings, *Geophysical Journal*
809 *International*, 189, 143–160, <https://doi.org/10.1111/j.1365-246X.2012.05378.x>, 2012.
- 810 Cowie, P. A., Phillips, R. J., Roberts, G. P., McCaffrey, K., Zijerveld, L. J. J., Gregory, L. C.,
811 Faure Walker, J., Wedmore, L. N. J., Dunai, T. J., Binnie, S. A., Freeman, S. P. H. T., Wilcken,
812 K., Shanks, R. P., Huismans, R. S., Papanikolaou, I., Michetti, A. M., and Wilkinson, M.:
813 Orogen-scale uplift in the central Italian Apennines drives episodic behaviour of earthquake
814 faults, *Sci Rep*, 7, 44858, <https://doi.org/10.1038/srep44858>, 2017.
- 815 D’Addezio, G., Pantosti, G., and Valensise, G.: Paleoearthquakes along the Irpinia fault at
816 Pantano di San Gregorio Magno (southern Italy), *Alpine and Mediterranean Quaternary*, 4,
817 121–136, 1991.



- 818 Delogkos, E., Howell, A., Seebeck, H., Shaw, B. E., Nicol, A., Mika Liao, Y.-W., and Walsh,
819 J. J.: Impact of Variable Fault Geometries and Slip Rates on Earthquake Catalogs From
820 Physics-Based Simulations of a Normal Fault, *Journal of Geophysical Research: Solid Earth*,
821 128, e2023JB026746, <https://doi.org/10.1029/2023JB026746>, 2023.
- 822 Dieterich, J. H.: Modeling of rock friction 1. Experimental results and constitutive equations,
823 *Journal of Geophysical Research: Solid Earth*, 84, 2161–2168,
824 <https://doi.org/10.1029/JB084iB05p02161>, 1979.
- 825 Dieterich, J. H. and Smith, D. E.: Nonplanar Faults: Mechanics of Slip and Off-fault Damage,
826 in: *Mechanics, Structure and Evolution of Fault Zones*, edited by: Ben-Zion, Y. and Sammis,
827 C., Birkhäuser, Basel, 1799–1815, https://doi.org/10.1007/978-3-0346-0138-2_12, 2010.
- 828 Doglioni, C.: Some remarks on the origin of foredeeps, *Tectonophysics*, 228, 1–20,
829 [https://doi.org/10.1016/0040-1951\(93\)90211-2](https://doi.org/10.1016/0040-1951(93)90211-2), 1993.
- 830 Erickson, B. A., Jiang, J., Barall, M., Lapusta, N., Dunham, E. M., Harris, R., Abrahams, L. S.,
831 Allison, K. L., Ampuero, J., Barbot, S., Cattania, C., Elbanna, A., Fialko, Y., Idini, B., Kozdon,
832 J. E., Lambert, V., Liu, Y., Luo, Y., Ma, X., Best McKay, M., Segall, P., Shi, P., van den Ende,
833 M., and Wei, M.: The Community Code Verification Exercise for Simulating Sequences of
834 Earthquakes and Aseismic Slip (SEAS), *Seismological Research Letters*, 91, 874–890,
835 <https://doi.org/10.1785/0220190248>, 2020.
- 836 Faure Walker, J. P.: *Mechanics of continental extension from Quaternary strain fields in the*
837 *Italian Apennines*, Doctoral, UCL (University College London), 405 pp., 2010.
- 838 Faure Walker, J. P., Roberts, G. P., Cowie, P. A., Papanikolaou, I. D., Sammonds, P. R.,
839 Michetti, A. M., and Phillips, R. J.: Horizontal strain-rates and throw-rates across breached
840 relay zones, central Italy: Implications for the preservation of throw deficits at points of normal
841 fault linkage, *Journal of Structural Geology*, 31, 1145–1160,
842 <https://doi.org/10.1016/j.jsg.2009.06.011>, 2009.
- 843 Faure Walker, J. P., Visini, F., Roberts, G., Galasso, C., McCaffrey, K., and Mildon, Z.:
844 Variable Fault Geometry Suggests Detailed Fault-Slip-Rate Profiles and Geometries Are
845 Needed for Fault-Based Probabilistic Seismic Hazard Assessment (PSHA), *Bulletin of the*
846 *Seismological Society of America*, 109, 110–123, <https://doi.org/10.1785/0120180137>, 2019a.
- 847 Faure Walker, J. P., Visini, F., Roberts, G., Galasso, C., McCaffrey, K., and Mildon, Z.:
848 Variable Fault Geometry Suggests Detailed Fault-Slip-Rate Profiles and Geometries Are
849 Needed for Fault-Based Probabilistic Seismic Hazard Assessment (PSHA), *Bulletin of the*
850 *Seismological Society of America*, 109, 110–123, <https://doi.org/10.1785/0120180137>, 2019b.
- 851 Faure Walker, J. P., Boncio, P., Pace, B., Roberts, G., Benedetti, L., Scotti, O., Visini, F., and
852 Peruzza, L.: Fault2SHA Central Apennines database and structuring active fault data for
853 seismic hazard assessment, *Sci Data*, 8, 87, <https://doi.org/10.1038/s41597-021-00868-0>, 2021.
- 854 Freed, A. M.: Earthquake Triggering by Static, Dynamic, and Postseismic Stress Transfer,
855 *Annual Review of Earth and Planetary Sciences*, 33, 335–367,
856 <https://doi.org/10.1146/annurev.earth.33.092203.122505>, 2005.



- 857 Frepoli, A., Maggi, C., Cimini, G. B., Marchetti, A., and Chiappini, M.: Seismotectonic of
858 Southern Apennines from recent passive seismic experiments, *Journal of Geodynamics*, 51,
859 110–124, <https://doi.org/10.1016/j.jog.2010.02.007>, 2011.
- 860 Galadini, F. and Galli, P.: Paleoseismology related to deformed archaeological remains in the
861 Fucino Plain. Implications for subrecent seismicity in Central Italy, *Annals of Geophysics*, 39,
862 <https://doi.org/10.4401/ag-4025>, 1996.
- 863 Galadini, F. and Galli, P.: The Holocene paleoearthquakes on the 1915 Avezzano earthquake
864 faults (central Italy): implications for active tectonics in the central Apennines, *Tectonophysics*,
865 308, 143–170, [https://doi.org/10.1016/S0040-1951\(99\)00091-8](https://doi.org/10.1016/S0040-1951(99)00091-8), 1999.
- 866 Galli, P.: Recurrence times of central-southern Apennine faults (Italy): Hints from
867 palaeoseismology, *Terra Nova*, 32, 399–407, <https://doi.org/10.1111/ter.12470>, 2020.
- 868 Galli, P. and Peronace, E.: New paleoseismic data from the Irpinia Fault. A different
869 seismogenic perspective for southern Apennines (Italy), *Earth-Science Reviews*, 136, 175–
870 201, <https://doi.org/10.1016/j.earscirev.2014.05.013>, 2014.
- 871 Galli, P., Bosi, V., Piscitelli, S., Giocoli, A., and Scionti, V.: Late Holocene earthquakes in
872 southern Apennine: paleoseismology of the Caggiano fault, *Int J Earth Sci (Geol Rundsch)*, 95,
873 855–870, <https://doi.org/10.1007/s00531-005-0066-2>, 2006.
- 874 Galli, P., Galadini, F., and Pantosti, D.: Twenty years of paleoseismology in Italy, *Earth-*
875 *Science Reviews*, 88, 89–117, <https://doi.org/10.1016/j.earscirev.2008.01.001>, 2008.
- 876 Galli, P., Giaccio, B., Peronace, E., and Messina, P.: Holocene Paleoeearthquakes and Early–
877 Late Pleistocene Slip Rate on the Sulmona Fault (Central Apennines, Italy), *Bulletin of the*
878 *Seismological Society of America*, 105, 1–13, <https://doi.org/10.1785/0120140029>, 2015.
- 879 Galli, P., Giaccio, B., Messina, P., and Peronace, E.: Three magnitude 7 earthquakes on a single
880 fault in central Italy in 1400 years, evidenced by new palaeoseismic results, *Terra Nova*, 28,
881 146–154, <https://doi.org/10.1111/ter.12202>, 2016.
- 882 Galli, P. A. C., Peronace, E., Quadrio, B., and Esposito, G.: Earthquake fingerprints along fault
883 scarps: A case study of the Irpinia 1980 earthquake fault (southern Apennines),
884 *Geomorphology*, 206, 97–106, <https://doi.org/10.1016/j.geomorph.2013.09.023>, 2014.
- 885 Galvez, P., Somerville, P., Petukhin, A., Ampuero, J.-P., and Peter, D.: Earthquake Cycle
886 Modelling of Multi-segmented Faults: Dynamic Rupture and Ground Motion Simulation of the
887 1992 Mw 7.3 Landers Earthquake, *Pure Appl. Geophys.*, 177, 2163–2179,
888 <https://doi.org/10.1007/s00024-019-02228-x>, 2020.
- 889 Gerstenberger, M. C., Marzocchi, W., Allen, T., Pagani, M., Adams, J., Danciu, L., Field, E.
890 H., Fujiwara, H., Luco, N., Ma, K. -F., Meletti, C., and Petersen, M. D.: Probabilistic Seismic
891 Hazard Analysis at Regional and National Scales: State of the Art and Future Challenges, *Rev.*
892 *Geophys.*, 58, <https://doi.org/10.1029/2019RG000653>, 2020.
- 893 Giardini, D., Basili, A., and Boschi, E.: Applying the relative hypocentre location approach:
894 where was the 1980 November 23 Irpinia earthquake?, *Geophysical Journal International*, 127,
895 605–615, <https://doi.org/10.1111/j.1365-246X.1996.tb04041.x>, 1996.



- 896 Gioia, D., Schiattarella, M., Mattei, M., and Nico, G.: Quantitative morphotectonics of the
897 Pliocene to Quaternary Auletta basin, southern Italy, *Geomorphology*, 134, 326–343,
898 <https://doi.org/10.1016/j.geomorph.2011.07.009>, 2011.
- 899 Guidoboni, E., Ferrari, G., Tarabusi, G., Sgattoni, G., Comastri, A., Mariotti, D., Ciuccarelli,
900 C., Bianchi, M. G., and Valensise, G.: CFTI5Med, the new release of the catalogue of strong
901 earthquakes in Italy and in the Mediterranean area, *Sci Data*, 6, 80,
902 <https://doi.org/10.1038/s41597-019-0091-9>, 2019.
- 903 Harris, R. A. and Simpson, R. W.: Suppression of large earthquakes by stress shadows: A
904 comparison of Coulomb and rate-and-state failure, *Journal of Geophysical Research: Solid*
905 *Earth*, 103, 24439–24451, <https://doi.org/10.1029/98JB00793>, 1998.
- 906 Heimisson, E. R.: Crack to pulse transition and magnitude statistics during earthquake cycles
907 on a self-similar rough fault, *Earth and Planetary Science Letters*, 537, 116202,
908 <https://doi.org/10.1016/j.epsl.2020.116202>, 2020.
- 909 Hillers, G., Mai, P. M., Ben-Zion, Y., and Ampuero, J.-P.: Statistical properties of seismicity
910 of fault zones at different evolutionary stages, *Geophysical Journal International*, 169, 515–
911 533, <https://doi.org/10.1111/j.1365-246X.2006.03275.x>, 2007.
- 912 Iacoletti, S., Cremen, G., and Galasso, C.: Advancements in multi-rupture time-dependent
913 seismic hazard modeling, including fault interaction, *Earth-Science Reviews*, 220, 103650,
914 <https://doi.org/10.1016/j.earscirev.2021.103650>, 2021.
- 915 Jiang, J., Erickson, B. A., Lambert, V. R., Ampuero, J.-P., Ando, R., Barbot, S. D., Cattania,
916 C., Zilio, L. D., Duan, B., Dunham, E. M., Gabriel, A.-A., Lapusta, N., Li, D., Li, M., Liu, D.,
917 Liu, Y., Ozawa, S., Pranger, C., and van Dinther, Y.: Community-Driven Code Comparisons
918 for Three-Dimensional Dynamic Modeling of Sequences of Earthquakes and Aseismic Slip,
919 *Journal of Geophysical Research: Solid Earth*, 127, e2021JB023519,
920 <https://doi.org/10.1029/2021JB023519>, 2022.
- 921 Jolivet, L., Faccenna, C., Goffé, B., Mattei, M., Rossetti, F., Brunet, C., Storti, F., Funicello,
922 R., Cadet, J. P., d’Agostino, N., and Parra, T.: Midcrustal shear zones in postorogenic
923 extension: Example from the northern Tyrrhenian Sea, *Journal of Geophysical Research: Solid*
924 *Earth*, 103, 12123–12160, <https://doi.org/10.1029/97JB03616>, 1998.
- 925 King, G. C. P., Stein, R. S., and Lin, J.: Static stress changes and the triggering of earthquakes,
926 *Bulletin of the Seismological Society of America*, 84, 935–953,
927 <https://doi.org/10.1785/BSSA0840030935>, 1994.
- 928 Lapusta, N., Rice, J. R., Ben-Zion, Y., and Zheng, G.: Elastodynamic analysis for slow tectonic
929 loading with spontaneous rupture episodes on faults with rate- and state-dependent friction,
930 *Journal of Geophysical Research: Solid Earth*, 105, 23765–23789,
931 <https://doi.org/10.1029/2000JB900250>, 2000.
- 932 Lombardi, A. M., Cinti, F. R., and Pantosti, D.: Paleoearthquakes modelling and effects of
933 uncertainties on probability assessment of next fault ruptures: the case of Central Italy surface
934 faulting earthquakes, *Geophysical Journal International*, 241, 1327–1347,
935 <https://doi.org/10.1093/gji/ggaf105>, 2025.



- 936 Luo, Y. and Ampuero, J.-P.: Stability of faults with heterogeneous friction properties and
937 effective normal stress, *Tectonophysics*, 733, 257–272,
938 <https://doi.org/10.1016/j.tecto.2017.11.006>, 2018.
- 939 Luo, Y., Ampuero, J. P., Galvez, P., Ende, M. van den, and Idini, B.: QDYN: a Quasi-
940 DYNamic earthquake simulator (v1.1), , <https://doi.org/10.5281/zenodo.322459>, 2017.
- 941 Marone, C.: Laboratory-Derived Friction Laws and Their Application to Seismic Faulting,
942 *Annual Review of Earth and Planetary Sciences*, 26, 643–696,
943 <https://doi.org/10.1146/annurev.earth.26.1.643>, 1998a.
- 944 Marone, C.: The effect of loading rate on static friction and the rate of fault healing during the
945 earthquake cycle, *Nature*, 391, 69–72, <https://doi.org/10.1038/34157>, 1998b.
- 946 Michetti, A. M., Brunamonte, F., Serva, L., and Vittori, E.: Trench investigations of the 1915
947 Fucino earthquake fault scarps (Abruzzo, central Italy): Geological evidence of large historical
948 events, *Journal of Geophysical Research: Solid Earth*, 101, 5921–5936,
949 <https://doi.org/10.1029/95JB02852>, 1996.
- 950 Mignan, A., Danciu, L., and Giardini, D.: Considering large earthquake clustering in seismic
951 risk analysis, *Nat Hazards*, 91, 149–172, <https://doi.org/10.1007/s11069-016-2549-9>, 2018.
- 952 Mildon, Z. K.: The link between earthquakes and structural geology; the role of elapsed time,
953 3D geometry and stress transfer in the central Apennines, Italy, 2017.
- 954 Mildon, Z. K., Roberts, G. P., Faure Walker, J. P., and Toda, S.: Coulomb pre-stress and fault
955 bends are ignored yet vital factors for earthquake triggering, *Nat. Commun.*, 1–9,
956 <https://doi.org/10.31223/osf.io/pt829>, 2019.
- 957 Mildon, Z. K., Roberts, G. P., Faure Walker, J. P., Beck, J., Papanikolaou, I., Michetti, A. M.,
958 Toda, S., Iezzi, F., Campbell, L., McCaffrey, K. J. W., Shanks, R., Sgambato, C., Robertson,
959 J., Meschis, M., and Vittori, E.: Surface faulting earthquake clustering controlled by fault and
960 shear-zone interactions, *Nat Commun*, 13, 7126, <https://doi.org/10.1038/s41467-022-34821-5>,
961 2022.
- 962 Milner, K. R., Shaw, B. E., Goulet, C. A., Richards-Dinger, K. B., Callaghan, S., Jordan, T.
963 H., Dieterich, J. H., and Field, E. H.: Toward Physics-Based Nonergodic PSHA: A Prototype
964 Fully Deterministic Seismic Hazard Model for Southern California, *Bulletin of the*
965 *Seismological Society of America*, 111, 898–915, <https://doi.org/10.1785/0120200216>, 2021.
- 966 Morewood, N. C. and Roberts, G. P.: The geometry, kinematics and rates of deformation within
967 an en échelon normal fault segment boundary, central Italy, *Journal of Structural Geology*, 22,
968 1027–1047, [https://doi.org/10.1016/S0191-8141\(00\)00030-4](https://doi.org/10.1016/S0191-8141(00)00030-4), 2000.
- 969 Mouslopoulou, V., Nicol, A., Howell, A., and Griffin, J. D.: Comparison of Paleoearthquake
970 Elapsed-Times and Mean Interevent-Times for a Global Data Set of Active Faults: Implications
971 for Future Earthquakes and Seismic Hazard, *Journal of Geophysical Research: Solid Earth*,
972 130, e2024JB030036, <https://doi.org/10.1029/2024JB030036>, 2025.
- 973 Nicol, A., Watterson, J., Walsh, J. J., and Childs, C.: The shapes, major axis orientations and
974 displacement patterns of fault surfaces, *Journal of Structural Geology*, 18, 235–248,
975 [https://doi.org/10.1016/S0191-8141\(96\)80047-2](https://doi.org/10.1016/S0191-8141(96)80047-2), 1996.



- 976 Nicol, A., Walsh, J., Berryman, K., and Nodder, S.: Growth of a normal fault by the
977 accumulation of slip over millions of years, *Journal of Structural Geology*, 27, 327–342,
978 <https://doi.org/10.1016/j.jsg.2004.09.002>, 2005.
- 979 Nicol, A., Robinson, R., Van Dissen, R., and Harvison, A.: Variability of recurrence interval
980 and single-event slip for surface-rupturing earthquakes in New Zealand, *New Zealand Journal*
981 *of Geology and Geophysics*, 59, 97–116, <https://doi.org/10.1080/00288306.2015.1127822>,
982 2016.
- 983 Okada, Y.: Internal deformation due to shear and tensile faults in a half-space, *Bulletin of the*
984 *Seismological Society of America*, 82, 1018–1040, <https://doi.org/10.1785/BSSA0820021018>,
985 1992.
- 986 Pace, B., Valentini, A., Ferranti, L., Vasta, M., Vassallo, M., Montagna, P., Colella, A., and
987 Pons-Branchu, E.: A Large Paleoeearthquake in the Central Apennines, Italy, Recorded by the
988 Collapse of a Cave Speleothem, *Tectonics*, 39, e2020TC006289,
989 <https://doi.org/10.1029/2020TC006289>, 2020.
- 990 Pantosti, D., Schwartz, D. P., and Valensise, G.: Paleoseismology along the 1980 surface
991 rupture of the Irpinia Fault: Implications for earthquake recurrence in the southern Apennines,
992 Italy, *Journal of Geophysical Research: Solid Earth*, 98, 6561–6577,
993 <https://doi.org/10.1029/92JB02277>, 1993.
- 994 Papanikolaou, I. D. and Roberts, G. P.: Geometry, kinematics and deformation rates along the
995 active normal fault system in the southern Apennines: Implications for fault growth, *Journal of*
996 *Structural Geology*, 29, 166–188, <https://doi.org/10.1016/j.jsg.2006.07.009>, 2007.
- 997 Papanikolaou, I. D., Roberts, G. P., and Michetti, A. M.: Fault scarps and deformation rates in
998 Lazio–Abruzzo, Central Italy: Comparison between geological fault slip-rate and GPS data,
999 *Tectonophysics*, 408, 147–176, <https://doi.org/10.1016/j.tecto.2005.05.043>, 2005.
- 1000 QGIS Development Team: QGIS Geographic Information System, Open Source Geospatial
1001 Foundation, 2009.
- 1002 Rice, J. R.: Spatio-temporal complexity of slip on a fault, *Journal of Geophysical Research:*
1003 *Solid Earth*, 98, 9885–9907, <https://doi.org/10.1029/93JB00191>, 1993.
- 1004 Rice, J. R. and Ben-Zion, Y.: Slip complexity in earthquake fault models., *Proceedings of the*
1005 *National Academy of Sciences*, 93, 3811–3818, <https://doi.org/10.1073/pnas.93.9.3811>, 1996.
- 1006 Roberts, G. P.: Fault orientation variations along the strike of active normal fault systems in
1007 Italy and Greece: Implications for predicting the orientations of subseismic-resolution faults in
1008 hydrocarbon reservoirs, *Bulletin*, 91, 1–20, <https://doi.org/10.1306/08300605146>, 2007.
- 1009 Roberts, G. P. and Michetti, A. M.: Spatial and temporal variations in growth rates along active
1010 normal fault systems: an example from The Lazio–Abruzzo Apennines, central Italy, *Journal*
1011 *of Structural Geology*, 26, 339–376, [https://doi.org/10.1016/S0191-8141\(03\)00103-2](https://doi.org/10.1016/S0191-8141(03)00103-2), 2004.
- 1012 Roberts, G. P., Sgambato, C., Mildon, Z. K., Iezzi, F., Beck, J., Robertson, J., Papanikolaou,
1013 I., Michetti, A. M., Faure Walker, J. P., Meschis, M., Shanks, R., Phillips, R., McCaffrey, K.
1014 J. W., Vittori, E., and Mitchell, S.: Spatial migration of temporal earthquake clusters driven by



- 1015 the transfer of differential stress between neighbouring fault/shear-zone structures, *Journal of*
1016 *Structural Geology*, 181, 105096, <https://doi.org/10.1016/j.jsg.2024.105096>, 2024.
- 1017 Roberts, G. P., Iezzi, F., Sgambato, C., Robertson, J., Beck, J., Mildon, Z. K., Papanikolaou,
1018 I., Michetti, A. M., Faure Walker, J., Mitchell, S., Meschis, M., Shanks, R., Phillips, R.,
1019 McCaffrey, K., Vittori, E., and Iqbal, M.: Characteristics and modelling of slip-rate variability
1020 and temporal earthquake clustering across a distributed network of active normal faults
1021 constrained by in situ ³⁶Cl cosmogenic dating of fault scarp exhumation, central Italy, *Journal*
1022 *of Structural Geology*, 195, 105391, 2025.
- 1023 Rodriguez Picada, C., Mildon, Z. K., van den Ende, M., Ampuero, J.-P., and Andrews, B. J.:
1024 Normal Fault Interactions in Seismic Cycles and the Impact of Fault Network Geometry,
1025 *Journal of Geophysical Research: Solid Earth*, 130, e2024JB030382,
1026 <https://doi.org/10.1029/2024JB030382>, 2025a.
- 1027 Rodriguez Picada, C., Mildon, Z., Yin, Y., and Galvez, P.: qdyn_hmat_lsoda: QDYN
1028 earthquake simulator with Hierarchical matrices and LSODA solver, ,
1029 <https://doi.org/10.5281/zenodo.17178002>, 2025b.
- 1030 Rodriguez Picada, C., Mildon, Z., Andrews, B., Yin, Y., Ampuero, J. P., van den Ende, M.,
1031 Sgambato, C., and Galvez, P.: Supplementary information 3D seismic cycle models of the
1032 Italian Apennines, <https://doi.org/10.5281/zenodo.17177111>, 2025c.
- 1033 Romanet, P., Bhat, H. S., Jolivet, R., and Madariaga, R.: Fast and Slow Slip Events Emerge
1034 Due to Fault Geometrical Complexity, *Geophysical Research Letters*, 45, 4809–4819,
1035 <https://doi.org/10.1029/2018GL077579>, 2018.
- 1036 Rovida, A., Locati, M., Camassi, R., Lolli, B., and Gasperini, P.: The Italian earthquake
1037 catalogue CPTI15, *Bull Earthquake Eng*, 18, 2953–2984, [https://doi.org/10.1007/s10518-020-](https://doi.org/10.1007/s10518-020-00818-y)
1038 00818-y, 2020.
- 1039 Rubin, A. M. and Ampuero, J.-P.: Earthquake nucleation on (aging) rate and state faults,
1040 *Journal of Geophysical Research: Solid Earth*, 110, <https://doi.org/10.1029/2005JB003686>,
1041 2005.
- 1042 Ruina, A.: Slip instability and state variable friction laws., *Journal of Geophysical Research*,
1043 88, 10359–10370, <https://doi.org/10.1029/JB088iB12p10359>, 1983.
- 1044 Savage, J. C.: A dislocation model of strain accumulation and release at a subduction zone, *J.*
1045 *Geophys. Res.*, 88, 4984–4996, <https://doi.org/10.1029/JB088iB06p04984>, 1983.
- 1046 Sgambato, C.: Variations in fault parameters and seismic hazard in the Central and Southern
1047 Italian Apennines, Doctoral, UCL (University College London), 522 pp., 2022.
- 1048 Sgambato, C., Faure Walker, J. P., Mildon, Z. K., and Roberts, G. P.: Stress loading history of
1049 earthquake faults influenced by fault/shear zone geometry and Coulomb pre-stress, *Sci Rep*,
1050 10, 12724, <https://doi.org/10.1038/s41598-020-69681-w>, 2020a.
- 1051 Sgambato, C., Faure Walker, J. P., and Roberts, G. P.: Uncertainty in strain-rate from field
1052 measurements of the geometry, rates and kinematics of active normal faults: Implications for
1053 seismic hazard assessment, *Journal of Structural Geology*, 131, 103934,
1054 <https://doi.org/10.1016/j.jsg.2019.103934>, 2020b.



- 1055 Sgambato, C., Faure Walker, J. P., Roberts, G. P., Mildon, Z. K., and Meschis, M.: Influence
1056 of Fault System Geometry and Slip Rates on the Relative Role of Coseismic and Interseismic
1057 Stresses on Earthquake Triggering and Recurrence Variability, *Journal of Geophysical*
1058 *Research: Solid Earth*, 128, e2023JB026496, <https://doi.org/10.1029/2023JB026496>, 2023.
- 1059 Sgambato, C., Roberts, G. P., Iezzi, F., Faure Walker, J. P., Beck, J., Mildon, Z. K., Michetti,
1060 A. M., Vittori, E., Robertson, J., Gheorghiu, D. M., and Shanks, R. P.: Millennial Slip-Rates
1061 Variability of Along-Strike Active Faults in the Italian Southern Apennines Revealed by
1062 Cosmogenic ³⁶Cl Dating of Fault Scarps, *Tectonics*, 44, e2024TC008529,
1063 <https://doi.org/10.1029/2024TC008529>, 2025.
- 1064 Shaw, B. E., Milner, K. R., Field, E. H., Richards-Dinger, K., Gilchrist, J. J., Dieterich, J. H.,
1065 and Jordan, T. H.: A physics-based earthquake simulator replicates seismic hazard statistics
1066 across California, *Science Advances*, 4, eaau0688, <https://doi.org/10.1126/sciadv.aau0688>,
1067 2018.
- 1068 Shaw, B. E., Fry, B., Nicol, A., Howell, A., and Gerstenberger, M.: An Earthquake Simulator
1069 for New Zealand, *Bulletin of the Seismological Society of America*, 112, 763–778,
1070 <https://doi.org/10.1785/0120210087>, 2022.
- 1071 Soliva, R., Benedicto, A., Schultz, R. A., Maerten, L., and Micarelli, L.: Displacement and
1072 interaction of normal fault segments branched at depth: Implications for fault growth and
1073 potential earthquake rupture size, *Journal of Structural Geology*, 30, 1288–1299,
1074 <https://doi.org/10.1016/j.jsg.2008.07.005>, 2008.
- 1075 Spagnuolo, E., Herrero, A., and Cultrera, G.: The effect of directivity in a PSHA framework,
1076 *Geophysical Journal International*, 191, 616–626, <https://doi.org/10.1111/j.1365-246X.2012.05630.x>, 2012.
- 1078 Stein, R. S.: The role of stress transfer in earthquake occurrence, *Nature*, 402, 605–609,
1079 <https://doi.org/10.1038/45144>, 1999.
- 1080 Stein, R. S., Barka, A. A., and Dieterich, J. H.: Progressive failure on the North Anatolian fault
1081 since 1939 by earthquake stress triggering, *Geophysical Journal International*, 128, 594–604,
1082 <https://doi.org/10.1111/j.1365-246X.1997.tb05321.x>, 1997.
- 1083 Thomas, M. Y., Lapusta, N., Noda, H., and Avouac, J.-P.: Quasi-dynamic versus fully dynamic
1084 simulations of earthquakes and aseismic slip with and without enhanced coseismic weakening,
1085 *Journal of Geophysical Research: Solid Earth*, 119, 1986–2004,
1086 <https://doi.org/10.1002/2013JB010615>, 2014.
- 1087 Thompson, E. M. and Worden, C. B.: Estimating Rupture Distances without a Rupture,
1088 *Bulletin of the Seismological Society of America*, 108, 371–379,
1089 <https://doi.org/10.1785/0120170174>, 2017.
- 1090 Toda, S., Stein, R. S., Reasenberg, P. A., Dieterich, J. H., and Yoshida, A.: Stress transferred
1091 by the 1995 M = 6.9 Kobe, Japan, shock: Effect on aftershocks and future earthquake
1092 probabilities, *Journal of Geophysical Research: Solid Earth*, 103, 24543–24565,
1093 <https://doi.org/10.1029/98JB00765>, 1998.



- 1094 Valentini, A., Visini, F., and Pace, B.: Integrating faults and past earthquakes into a
1095 probabilistic seismic hazard model for peninsular Italy, *Natural Hazards and Earth System*
1096 *Sciences*, 17, 2017–2039, <https://doi.org/10.5194/nhess-17-2017-2017>, 2017.
- 1097 Wells, D. L. and Coppersmith, K. J.: New empirical relationships among magnitude, rupture
1098 length, rupture width, rupture area, and surface displacement, *Bulletin of the Seismological*
1099 *Society of America*, 84, 974–1002, <https://doi.org/10.1785/BSSA0840040974>, 1994.
- 1100 Westaway, R.: Quaternary uplift of southern Italy, *Journal of Geophysical Research: Solid*
1101 *Earth*, 98, 21741–21772, <https://doi.org/10.1029/93JB01566>, 1993.
- 1102 Westaway, R. and Jackson, J.: The earthquake of 1980 November 23 in Campania—Basilicata
1103 (southern Italy), *Geophysical Journal International*, 90, 375–443,
1104 <https://doi.org/10.1111/j.1365-246X.1987.tb00733.x>, 1987.
- 1105 Yin, Y.: Seismicity and fault interaction through observation and simulation, *ETH Zurich*,
1106 <https://doi.org/10.3929/ETHZ-B-000578638>, 2022.
- 1107 Yin, Y., Galvez, P., Heimisson, E. R., and Wiemer, S.: The role of three-dimensional fault
1108 interactions in creating complex seismic sequences, *Earth and Planetary Science Letters*, 606,
1109 118056, <https://doi.org/10.1016/j.epsl.2023.118056>, 2023.
- 1110
- 1111